NATIONAL BUREAU OF STANDARDS

NBS TECHNICAL NOTE 1151

U.S. DEPARTMENT OF COMMERCE / National Bureau of Standards

Surface Roughness Measurements of Circular Disks and Their Correlation with Hydrodynamic Drag

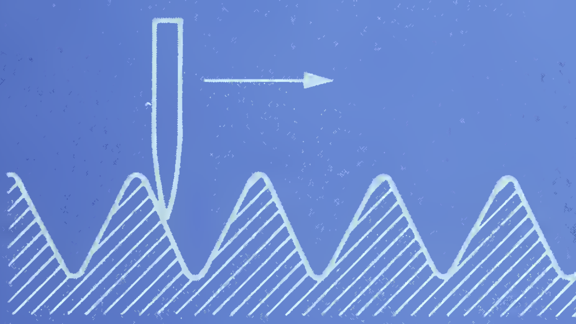

NATIONAL BUREAU OF STANDARDS

The National Bureau of Standards[1] was established by an act of Congress on March 3, 1901. The Bureau's overall goal is to strengthen and advance the Nation's science and technology and facilitate their effective application for public benefit. To this end, the Bureau conducts research and provides: (1) a basis for the Nation's physical measurement system, (2) scientific and technological services for industry and government, (3) a technical basis for equity in trade, and (4) technical services to promote public safety. The Bureau's technical work is performed by the National Measurement Laboratory, the National Engineering Laboratory, and the Institute for Computer Sciences and Technology.

THE NATIONAL MEASUREMENT LABORATORY provides the national system of physical and chemical and materials measurement; coordinates the system with measurement systems of other nations and furnishes essential services leading to accurate and uniform physical and chemical measurement throughout the Nation's scientific community, industry, and commerce; conducts materials research leading to improved methods of measurement, standards, and data on the properties of materials needed by industry, commerce, educational institutions, and Government; provides advisory and research services to other Government agencies; develops, produces, and distributes Standard Reference Materials; and provides calibration services. The Laboratory consists of the following centers:

Absolute Physical Quantities[2] — Radiation Research — Thermodynamics and Molecular Science — Analytical Chemistry — Materials Science.

THE NATIONAL ENGINEERING LABORATORY provides technology and technical services to the public and private sectors to address national needs and to solve national problems; conducts research in engineering and applied science in support of these efforts; builds and maintains competence in the necessary disciplines required to carry out this research and technical service; develops engineering data and measurement capabilities; provides engineering measurement traceability services; develops test methods and proposes engineering standards and code changes; develops and proposes new engineering practices; and develops and improves mechanisms to transfer results of its research to the ultimate user. The Laboratory consists of the following centers:

Applied Mathematics — Electronics and Electrical Engineering[2] — Mechanical Engineering and Process Technology[2] — Building Technology — Fire Research — Consumer Product Technology — Field Methods.

THE INSTITUTE FOR COMPUTER SCIENCES AND TECHNOLOGY conducts research and provides scientific and technical services to aid Federal agencies in the selection, acquisition, application, and use of computer technology to improve effectiveness and economy in Government operations in accordance with Public Law 89-306 (40 U.S.C. 759), relevant Executive Orders, and other directives; carries out this mission by managing the Federal Information Processing Standards Program, developing Federal ADP standards guidelines, and managing Federal participation in ADP voluntary standardization activities; provides scientific and technological advisory services and assistance to Federal agencies; and provides the technical foundation for computer-related policies of the Federal Government. The Institute consists of the following centers:

Programming Science and Technology — Computer Systems Engineering.

[1]Headquarters and Laboratories at Gaithersburg, MD, unless otherwise noted; mailing address Washington, DC 20234.
[2]Some divisions within the center are located at Boulder, CO 80303.

Surface Roughness Measurements of Circular Disks and Their Correlation with Hydrodynamic Drag

T. V. Vorburger
F. E. Scire
E. C. Teague

Center for Manufacturing Engineering
National Engineering Laboratory
National Bureau of Standards
Washington, DC 20234

Sponsored in part by:
David Taylor Naval Ship Research and Development Center
Annapolis, MD 21402

U.S. DEPARTMENT OF COMMERCE, Malcolm Baldrige, Secretary
NATIONAL BUREAU OF STANDARDS, Ernest Ambler, Director

Issued January 1982

National Bureau of Standards Technical Note 1151
Nat. Bur. Stand. (U.S.), Tech. Note 1151, 63 pages (Jan. 1982)
CODEN: NBTNAE

U.S. GOVERNMENT PRINTING OFFICE
WASHINGTON: 1982

Abstract

The problem of relating hull roughness to the drag of ships is a complex and important one in ship research. One of the complications is that there are three fairly distinct roughness regimes (microroughness, macroroughness, and structural roughness) which make up a ship's surface and their relative importance is not yet well understood. The present report focuses on stylus measurements of the microroughness of rotating disks and their significant correlation with drag measurements. In particular, the roughest disks had drag coefficients C_m that were $\sim$ 30 percent greater than those of the smoothest disks. The following empirical formula was derived to relate C_m with the roughness average R_a and the peak-count wavelength λ_{pc} at a Reynold's number of 1.5×10^6.

$$C_m = b\ R_a/(\lambda_{pc})^{1/2} + C_o,$$

where $b = 3.85 \pm 0.22 \times 10^{-3}\ \mu m^{-1/2}$ and $C_o = 6.48 \pm 0.07 \times 10^{-3}$. The formula was observed to hold for both painted and bare metal disks.

Key words: disks; drag; flow; friction disk; hulls; hydrodynamic drag; rotating disk; roughness; ships; stylus; surface roughness; surface topography.

TABLE OF CONTENTS

Executive Summary

The problem of relating hull roughness to the drag of ships is a complex and important one in ship research. One of the complications is that there are three fairly distinct roughness regimes (microroughness, macroroughness, and structural roughness) which make up a ship's surface, and their relative contributions to ship drag is not yet well understood. The microroughness regime is caused primarily by machining marks and paint texture; macroroughness is mainly due to inhomogeneities in the paint application, to corrosion, and to paint flaking; and structural roughness consists of large-scale perturbations such as plate warping or metal joining imperfections. The present report focuses on stylus measurements of the microroughness of test rotating disks performed at the NBS and the correlation of these data with drag measurements performed by the David Taylor Naval Ship Research and Development Center (DTNSRDC). The report discusses the effects of roughness wavelength as well as roughness amplitude on drag. The key findings demonstrate that under the present experimental conditions the roughness average R_a and the peak-count wavelength λ_{pc} are related to the drag coefficient C_m of the rotating disks as shown in the figure. Thus, the roughest disks were found to have drag coefficients that are about 30 percent greater than those of the smoothest

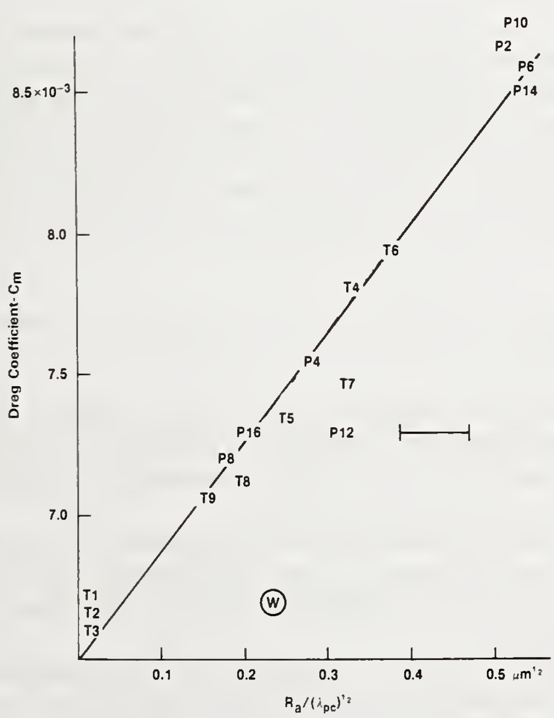

disks. Based on a statistical analysis of the data, the following empirical relationship between C_m, R_a, and λ_{pc} for a Reynold's number of 1.5×10^6 was obtained:

$$C_m = bR_a/(\lambda_{pc})^{1/2} + C_o,$$

where $b = 3.85 \pm 0.22 \times 10^{-3}\ \mu m^{-1/2}$ and $C_o = 6.48 \pm 0.07 \times 10^{-3}$.

The disks that were used for this study were all of uniform size and shape, but their surfaces were produced by two different manufacturing processes. One important result was that the above formula could be used to predict C_m for both sets of disks. The first was a set of nine bare titanium alloy disks. Three of these were finished by a lapping process and were quite smooth with R_a's ranging from 0.14 to 0.17 μm. The other six were finished by end milling with a V-shaped tool. They exhibited roughness patterns that were grid like and highly periodic with R_a's ranging from ~5 to 16 μm. The second set consisted of eight painted disks, all of which had random, gritty surface finishes characteristic of the paints themselves. Four different combinations of paint systems were used on these disks and they produced four different surface finishes.

In addition to R_a and λ_{pc}, the other surface parameters and functions computed from stylus measurements were the peak-to-valley roughness R_{max}, the peak-to-valley waviness W_{max}, the average slope S_a, the root mean square roughness R_q, the average wavelength λ_a, the amplitude density function, the autocorrelation function, and the power spectral density. All of the results for the above parameters and typical graphs for the functions are given in the accompanying report.

During the course of this work, we arrived at a number of conclusions as outlined below:

- At present, it seems that knowledge of one amplitude-sensitive parameter and one wavelength-sensitive parameter is adequate for characterizing increases in the drag of rotating disks due to surface roughness.
- R_a is the preferred amplitude-sensitive parameter because it is the most widely used. We propose λ_{pc} as the wavelength parameter because it is sensitive to the larger profile features rather than to the fine structure.
- There is a need for all workers in the field to standardize on measuring the same parameters so that the results of one group can be more easily related to the work of other groups.
- The three dimensional structure of a surface is not so important in the drag problem as the two dimensional profile along the direction of flow.

- The overall waviness (warp) of the disks does not seem to affect their drag characteristics.
- Soaking the disks in salt water over the course of 2 weeks did very little to affect their R_a values.
- Both the painting and machining processes were fairly uniform since the differences between the measured R_a of the front and back surfaces or between pairs of the same set were not significant.
- The ratio between R_{max} and R_a depended on whether the surfaces were lapped, milled, or painted.

1. Introduction

Surface roughness increases the hydrodynamic drag on ships. Hence, a rough hull surface causes both a loss in ship speed for a given input power and a waste of fuel. This report discusses recent state-of-the-art measurements of surface roughness parameters and their correlation with results of drag experiments. It is part of a larger investigation by the Navy to understand better the effects of roughness upon drag and to improve the speed and efficiency of high-speed ships.

1.1 Basic Ideas in Hydrodynamics and Ship Research

The drag of a body moving through a fluid is the force required to keep the body moving at constant speed. For a ship in water, the drag consists of four components: skin-friction, form drag, wave making, and air resistance [1,2]. The last three do not depend significantly upon hull roughness. The skin-friction, on the other hand, is caused by the tangential shear stresses exerted by the water on the moving hull surface, and its magnitude depends strongly on the hull roughness as well as several other factors including the speed of the ship, its length and surface area, and the density and viscosity of the water. As water flows past a ship there is a thin sublayer adjacent to the hull in which the flow is laminar. As long as the surface roughness heights are smaller than the thickness δ_o of the laminar sublayer, the ship is considered to be hydrodynamically smooth and the flow is not affected by the roughness. However, for roughness heights greater than δ_o, the skin-friction increases rapidly with roughness. For a large ship moving at a speed of 15 m/sec (30 knots), δ_o is approximately 7 μm [3]. Typical ships, however, have peak-to-valley roughnesses an order of magnitude larger than this, resulting in perhaps a 40 percent or more loss of power with respect to that for a ship with a smooth hull [1].

Hull roughness is increased by the corrosion and fouling processes in the marine environment. To reduce these effects, paint coatings are applied to the hulls of both commercial ships and warships. In general, anticorrosive (AC) coatings are applied first, followed by antifouling (AF) top coats. Several factors, therefore, contribute to the roughness of ships. First of all there is the basic texture of the coating itself. Then there are factors in the coating process including poor surface preparation and uneven application. Finally, the original coatings are slowly degraded by corrosion and fouling. Indeed, the marine environment is so severe that the peak-to-valley roughness of commercial ships can reach 500 μm or more [1]. However, even new coatings can have peak-to-valley roughnesses of 45 μm or more, several times the thickness of a hydrodynamically smooth surface [4]. Therefore, the Navy's program to improve the speed of ships seeks to develop coatings that will have (1) smoother texture so that the condition of hydrodynamic smoothness is approached, and (2) better AC and AF properties to reduce the degradation of the surfaces of ships in service.

1.2 Scope of the Present Report

In this report we discuss the roughness of fresh coatings. One question that needs to be answered is whether this part of the problem is significant in view of the severe degradation problem associated with corrosion and fouling. Unfortunately, because of the extreme complexity of the problem, it is next to impossible to predict the skin friction of a ship simply from a knowledge of hull shape and surface roughness parameters. On the other hand, experiments to measure the drag of full-scale ships with various coating systems are prohibitively expensive. Therefore, the Navy has taken recourse to small-scale drag experiments using rotating disks with various painted and bare metal surfaces. The experiments seek to correlate roughness parameters of the disks (measured by NBS) with drag measurements (by DTNSRDC) in a rotating disk instrument. It may then be possible to scale up the results to predict the drag of real ships [5].

The focus of the NBS work is threefold:
1) to measure the roughness parameters of a series of circular disks with various painted and bare metal surfaces,
2) to correlate these results with measurements of drag and, thereby, to determine those roughness parameters important to hull drag, and
3) to develop adequate statistical procedures for the measurement and analysis of roughness data.

Section 2 contains a general discussion of roughness measurement and its application to hull surfaces. Sections 3-6 deal with the NBS roughness and waviness measurements of the disks, and section 7 deals with the data analysis of these measurements and the correlation with Navy drag measurements. Section 8 contains our conclusions and recommendations.

2. Surface Roughness Measurement

The goal of surface roughness measurement in ship research is to understand the complex relationship between the surface topography and the skin friction well enough so that one could measure a few surface topographic parameters on a ship and predict the effects on drag. In the ideal situation, one would know which surface parameters to measure and would have an instrument for making high-speed measurements over a relatively large area of the ship's surface, in situ, either in drydock or underwater. There are, however, great limitations in our knowledge of hull surface topography and its effects on skin friction and in our ability to make economical, thorough measurements. A short review of the history and limitations of surface roughness measurement in ship research is given in the following subsections.

2.1 Roughness Regimes

The roughness of ships may be divided into three regimes: microroughness, macroroughness, and structural roughness [6]. In general,

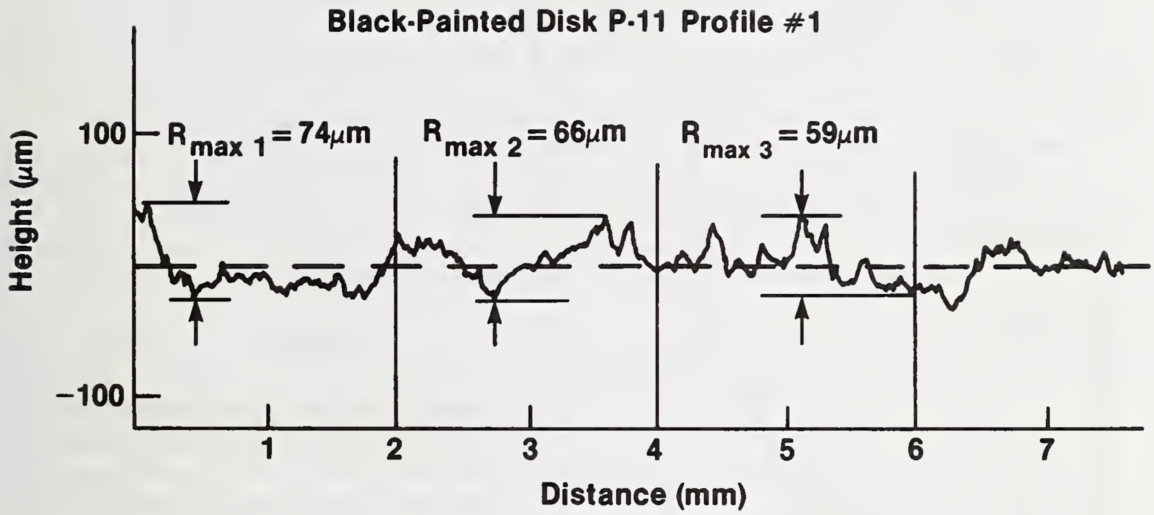

Figure 1. Typical surface profile for a circular disk fabricated at the Naval Ship Research and Development Center. The profile has been arbitrarily broken up into 2-mm sampling lengths and the maximum peak-to-valley-roughness R_{max} has been calculated for each. The mean line is represented by the dotted line.

each of these roughness regimes is caused by different processes and each merits study independently of the others. The microroughness is caused primarily by machining scratches and marks due to tool vibration and feed, paint texture, or, in the case of replicas, the texture of the material itself. The macroroughness is mainly due to inhomogeneities in the paint application, corrosion, and paint flaking. Structural roughness consists of large scale perturbations on the ideal form of the object. For a ship hull, it includes plate warping, rivet heads, large weld beads, and the edges of openings. For a rotating disk, the structural roughness is primarily the warp of the disk, but it may involve other long-scale errors of form as well.

These regimes may be roughly classified in terms of the characteristic distances between peaks and valleys along the surface. This procedure is begun by Fourier decomposition of the surface profile (e.g., fig. 1) into sinusoidal component wavelengths. When this is done for an object such as a large flat plate being tested for drag, the resulting power spectral density (PSD) looks like that in figure 2 [7]. In general, the microroughness regime spans surface wavelengths on the order of a few mm or less, the macroroughness extends from several mm to several tens of mm, and the structural roughness extends from there up to approximately several meters. In figure 2, the value of the PSD at a particular wavelength is proportional to the square of the amplitude of each Fourier component in the profile. It is important

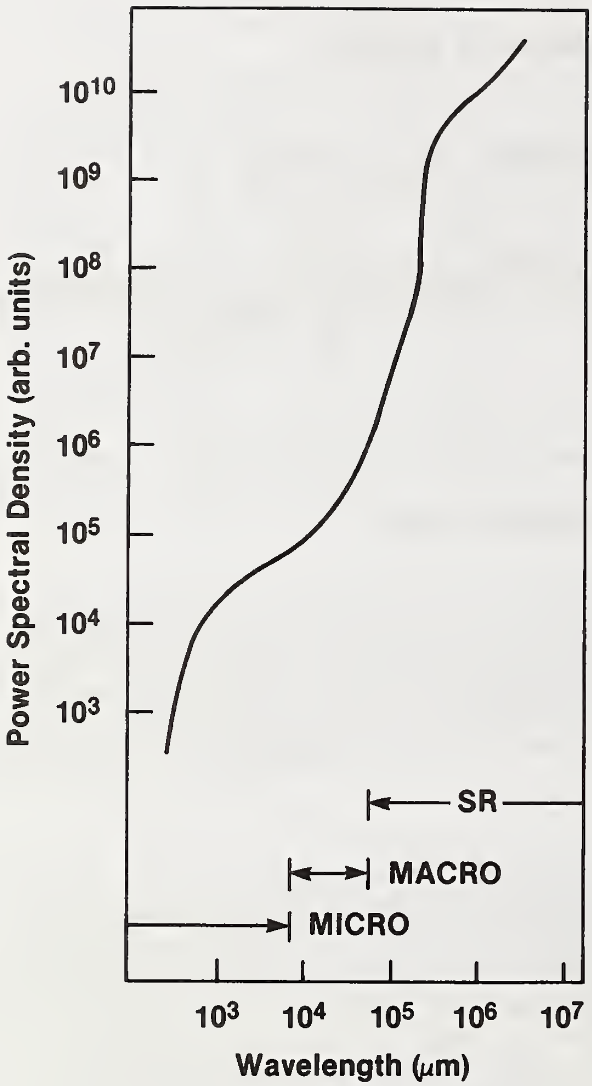

Figure 2.

Power Spectral Density of a 20 m length of primer-coated ship's plate resting in the bottom of a flow channel. The approximate wavelength ranges of the microroughness, macro-roughness, and structural roughness regimes are also shown. The curve (taken from Ref. 7) was pieced together from measurements made with three instruments: stylus instrument, dial gauge and straight-edge, and electronic level.

to note that the long-wavelength surface features are generally higher in amplitude than the short-wavelength features [7]. It seems then that a key problem in ship research is whether the smaller, more closely spaced surface features contribute more or less to the drag than the larger, more widely spaced features, i.e., whether one of these regimes dominates over the others in affecting drag.

2.2 Stylus Instruments

The standard technique for surface topography measurement has been the stylus technique [8]. This instrument (see fig. 3) uses a fine diamond stylus, which is traversed over the surface, and a transducer which produces a time-varying, electrical signal that, under the proper conditions, accurately represents the undulations of the surface profile. The resulting data may then be digitized, stored in a computer [8-10], and conveniently analyzed to yield a wide variety of statistical parameters and functions [7-15] for characterizing the surface. Stylus data are therefore accurate, quantitative, and analyzable.

Resolution and range are also strong features of stylus instruments. The ultimate vertical resolution (given by the rms noise of the instrument) can be as small as 0.1 nm [16] and the range can be as high as 100 μm. The horizontal resolution is limited by the stylus tip width [17-18]. It is typically several micrometers, but can be as small as 0.1 μm, more than acceptable for most topographic measurements.

However, the conventional stylus instrument has a number of shortcomings. The transducer and the stylus tips are fragile, so the instrument must be used in a fairly quiet, clean environment. A surface profile measurement takes several seconds, a bit on the slow side for some applications. Finally, the instrument generates two-dimensional surface profiles rather than three-dimensional surface contour maps. Therefore, the fraction of the surface area examined by the technique is vanishingly small. Briefly then, the stylus is fragile and slow, and under normal usage it produces only two-dimensional data. The foregoing limit its usefulness for quality inspection of ship surfaces in drydock and for measurements of ship hulls underwater.

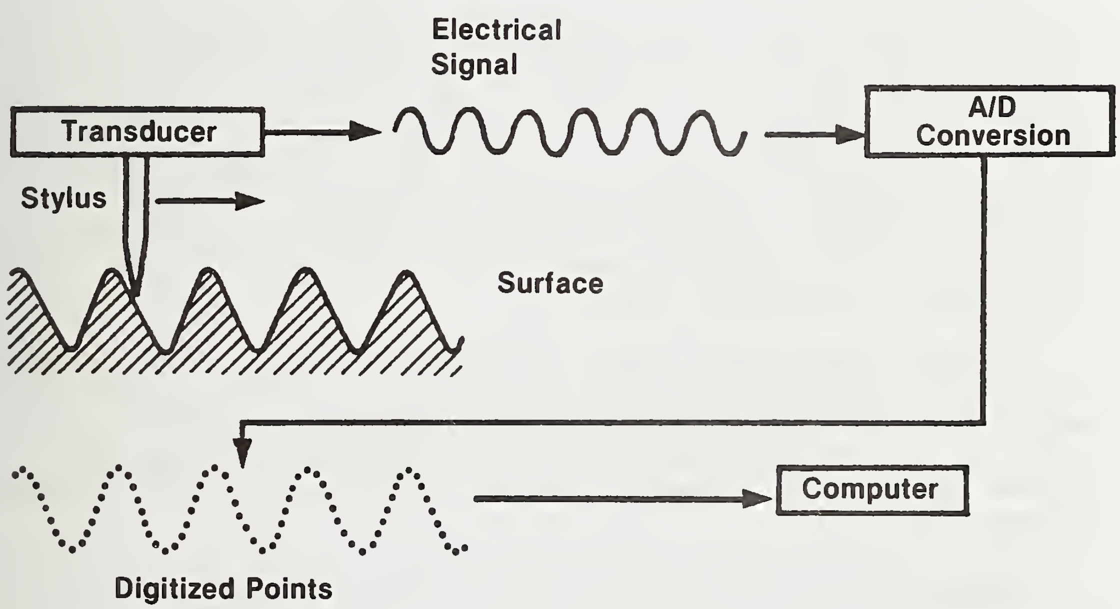

Figure 3. Schematic diagram of a stylus instrument for surface roughness measurements

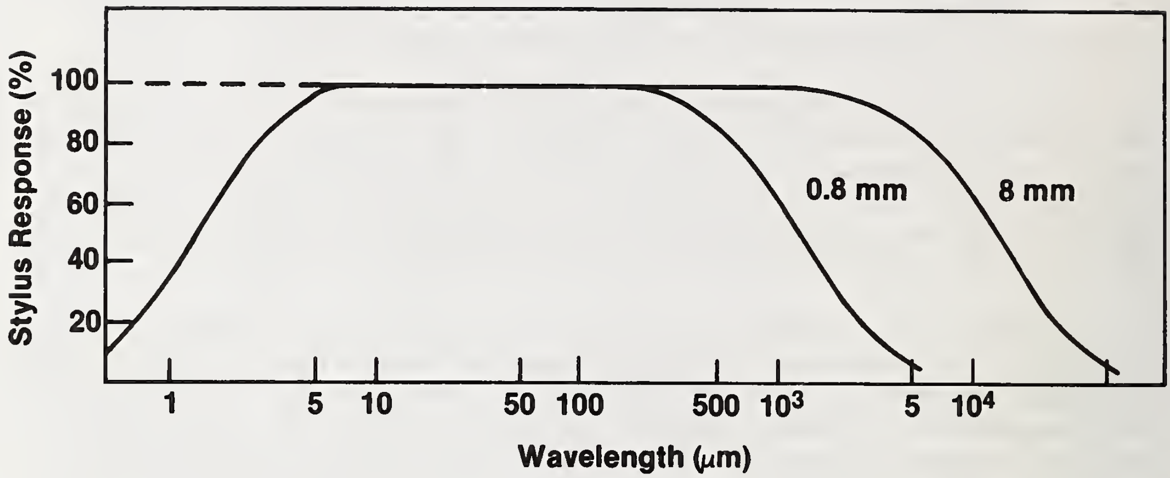

Figure 4. Typical response function for a stylus instrument. The response is limited at lower wavelengths by the stylus radius and at higher wavelengths by an electronic filter or by the trace length itself. Response curves for filters with 0.8 and 8 mm cutoffs are shown.

The British Ship Research Association (BSRA) manufactures a portable, and more robust, stylus instrument called the electronic hull roughness analyzer, which features a large vertical range for measuring the extremely rough surfaces typical of ship hulls. A similar instrument, called the monotester, is manufactured in Norway. The drawback of these instruments is that they output only one parameter, the peak-to-valley roughness. Otherwise these instruments are every bit as slow as conventional stylus instruments. Since at least 50 profiles are required for an adequate check of hull roughness [19], the measurement process can be quite expensive.

There is then a need for an instrument capable of rapid, in situ measurements. Optical, microwave, and ultrasonic techniques offer perhaps the greatest potential along these lines, but a great deal of research and development must be done to establish the connections between the parameters measured by these techniques and hull roughness parameters.

2.3 Instrument Bandwidth

In all forms of surface roughness measurement, however, one must take into account the approximate bandwidth of the probe, i.e., the approximate range of surface spacings or wavelengths which it senses. Stylus instruments are typically sensitive to the range of wavelengths extending from about 1 μm to about 10 mm. This range is limited at the lower end by the finite size of the stylus tip and at the upper end by the sampling length, which in turn is usually determined by an electronic filter with specified cutoff length. A schematic plot of a typical stylus instrument's response vs. wavelength is shown in figure 4 [15]. The curves show the characteristics of two filters available with many stylus instruments. These have nominal cutoff lengths of 0.8 and 8 mm. In the absence of an electronic filter, the upper end of the sensitive band is limited ultimately by the traverse length of the instrument, but that limit may be reduced by graphical division of the profile into sections. For example, figure 1 shows a roughness profile broken into 2-mm sampling lengths with the maximum peak-to-valley roughness calculated for each.

The choice of sampling length greatly influences the measured values of roughness parameters. This is particularly true because roughness generally increases with surface wavelength [7], as shown in figure 2 and elsewhere [12], and the longest wavelengths within the sampling length tend to dominate the roughness measurement. For example, the peak-to-valley parameter calculated in figure 1 is sensitive neither to the larger features of the surface profile with wavelength greater than 2 mm nor to the very fine features, but rather to surface wavelengths on the order of a millimeter. The choice of sampling length therefore implies a choice of which regime is most significant to the function of the surface. In many industrial applications the standard sampling length is 0.8 mm. However, for hull roughness measurement a longer scale is required. The BSRA has traditionally chosen 50 mm as the standard sampling length [19], but the present report is primarily concerned with the finer surface texture. Therefore, since a standard electronic cutoff of 8 mm lies close to the upper end of the microroughness regime and near the lower end of the macroroughness regime, it becomes convenient to redefine these regimes in terms of the sampling length. Henceforward in this report, the microroughness will be defined as those surface structures which can be measured by an instrument with a sampling length of ~8 mm, and the macroroughness will be those structures with longer wavelengths which can be measured using a 50-mm sampling length. This definition makes the macroroughness regime equivalent to the regime traditionally measured by the BSRA methods. Structural roughness will consist of surface wavelengths greater than 50 mm, plus any imperfections caused by metal joining, such as protruding fasteners or weld beads.

2.4 Roughness Parameters

Once the surface profile has been measured, the question arises as to which of the many parameters most directly affect surface drag. Although many different parameters have been defined to characterize surfaces, we will introduce only those considered most relevant in the present discussion. Additional information on surface parameters may be found elsewhere [7-15]. There are basically three kinds of roughness parameters: amplitude parameters, wavelength parameters, and hybrid parameters which are sensitive to both amplitude and wavelength.

2.4.1 Amplitude Parameters

In all forms of roughness measurement, amplitude parameters are considered to be most important. This is true in ship research as well, since there is a definite correlation between roughness amplitude and drag [1]. Indeed, an often-used rule of thumb is that ships consume approximately 2.5 percent more power to maintain a constant speed for every 25 μm increase in the roughness mean apparent amplitude (M.A.A.) [19]. We discuss M.A.A. as well as some of the other more important roughness parameters below.

a) Roughness Average-R_a. This parameter is also known as the center line average (CLA) or the arithmetic average (AA), but R_a is now the internationally standardized nomenclature [15]. R_a represents the average absolute deviation of the profile about its mean line, and it is defined as follows:

$$R_a = (1/L)\int_0^L |y(x)|\,dx, \qquad (1)$$

where x is the distance along the surface, y(x) defines the height of the surface profile about the mean line (fig. 1), and L is the sampling length. For a digital instrument, like the one at NBS, which represents a surface profile by N equally spaced digitized points y_i, the definition becomes

$$R_a = (1/N)\sum_{i=1}^{N} |y_i|. \qquad (2)$$

R_a is the most widely used surface parameter in the world, partly because it is an easy one to calculate. All commercial stylus instruments that we know of, except the two manufactured specifically for hull measurements, have direct readouts of the R_a value.

b) RMS Roughness - R_q. This parameter, also known as σ in the optics and statistics communities, is defined by

$$R_q = \left[(1/L) \int_0^L y^2(x)\, dx \right]^{1/2} \quad , \qquad (3)$$

or in the case of a digitized profile by

$$R_q = \left[(1/N) \sum_{i=1}^{N} y_i^{\,2} \right]^{1/2} \quad . \qquad (4)$$

Since R_q is equal to one standard deviation of the profile about the mean line, a number of theoretical calculations of surface properties yield results which are naturally expressed in terms of R_q rather than R_a. It is therefore a parameter more widely used than R_a in theoretical work. R_q is always greater than or equal to R_a.

c) Maximum Peak-to-Valley Roughness - R_{max}. This parameter is defined as the height difference between the highest peak and the lowest valley on the profile within the sampling length. When the surface profile contains more than one sampling length (fig. 1), the R_{max} value is generally calculated as the average of the results obtained for the several sampling lengths. Discussion of this parameter poses the important question of whether R_a or R_{max} is more significant to the surface drag problem, i.e. whether the flow over the surface is more sensitive to the highest peaks and lowest valleys or to some average property of all the peaks and valleys. The BSRA and Norwegian instruments yield values for this parameter and none other. A schematic diagram of a surface profile and the parameters R_a, R_q, and R_{max} is shown in figure 5.

d) Mean Apparent Amplitude - M.A.A. This parameter was traditionally used by the BSRA when manual methods were used to calculate roughness. It was obtained by dividing the profile into 50-mm sampling lengths, drawing envelope curves through the peaks and valleys of the surface profile, and calculating the enclosed area per 50-mm sampling length. With the advent of the BSRA's own electronic hull roughness analyzer, which yields R_{max} instead of M.A.A., this parameter is probably obsolete.

e) Equivalent Sand Grain - K_s. In the 1930's, Nikuradse [20] performed important experiments on the flow resistance of pipes which had been roughened by cementing sand grains of various diameters to the walls. Since his results for roughness were expressed in terms of grain sizes K_s, there has been some interest in expressing other forms of roughness measurements in terms of the equivalent sand grain roughness [20-22] to take advantage of his results for flow resistance. However, we do not

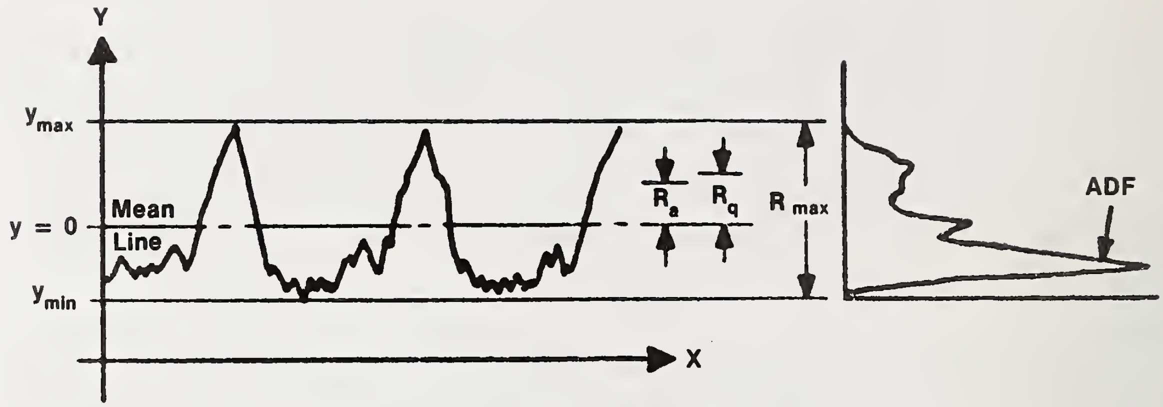

Figure 5. Schematic surface profile y(x) showing several roughness height parameters and the amplitude density function (ADF).

pursue that approach in the present work.

f) The Need for Standardization. From the above it seems apparent that expedience has ruled the choices of roughness parameters in the past. Theoreticians and statisticians tend to use R_q. Nikuradse, on the other hand, probably chose K_s because that was the easiest parameter to control and measure. The BSRA used M.A.A. when their calculations were done manually, but now with the electronic instrument their parameter of choice seems to be R_{max} instead. Because the conversions from one parameter to another vary from one type of surface to another, it is difficult to compare the findings of different groups when they have measured different parameters. There is a clear need for workers in the field of surface drag to standardize on measuring at least one height parameter that is the same for all, and functionally it may not matter a great deal which one. R_a is currently the most popular with engineers, and therefore, would enable workers in the field of ship research to communicate their needs more easily with engineers and scientists outside the field. There is, however, the possibility that other parameters, particularly R_{max}, may be more significant in drag. In this paper we consider both R_a and R_{max} as alternative roughness amplitude parameters to be correlated with the results of drag experiments on friction disks.

2.4.2 Wavelength Parameters

Surface wavelength effects on drag have not been studied as much as roughness amplitudes. However, Schlichting [20] has shown experimentally that the spacing between asperities on the inner walls of pipes affects the flow resistance of the pipes. There should be similar effects due to asperity spacing on ship hulls as well. Three of the wavelength parameters that can be used to characterize spacings are discussed below.

a) Average Wavelength - λ_a. Spragg and Whitehouse [23] first proposed this parameter to answer the need in the manufacturing industry to characterize spacings. It is defined by

$$\lambda_a = 2\pi R_a / S_a, \tag{5}$$

where S_a is the average slope of the surface profile (to be discussed below). The wavelength of a perfect sine wave is exactly equal to λ_a as obtained from the above formula. For random surfaces, λ_a tends to be more sensitive to the shorter wavelength components within each sampling length, whereas it is felt that surface drag should depend on the larger, longer wavelength surface features.

The average slope S_a is a hybrid parameter since it is sensitive to both roughness and wavelength. We define S_a for a digitized profile by

$$S_a = (1/Pk\tau) \sum_{j=1,1+k,1+2k,\ldots}^{1+Pk} |y_{j+k} - y_j|, \tag{6}$$

where τ is the horizontal point spacing of the digitized profile and $k\tau$ is the horizontal point spacing that determines the resolution of the calculation. The quantity $k\tau$ is equal to an integral number of point spacings of the profile itself and P is the total number of these $k\tau$ spacings in the profile. The numerical value of S_a depends on the resolution of the instrument and on the spacing $k\tau$ [8]. In the present work, $k\tau$ is chosen to be 7.6 μm, approximately equal to the stylus radius.

b) Peak-Count Wavelength - λ_{pc}. To address the need to measure the longer wavelengths, we have defined the quantity λ_{pc} which is similar to the peakcount parameter occasionally used in industry [24]. As shown in figure 6, λ_{pc} is defined as twice the trace length divided by the number of times that the profile crosses completely through a mean band centered about the mean line. The height of the mean band is rather arbitrary. For the present measurements we have chosen a band height equal to the measured R_a of the profile.

c) Autocorrelation Length - α. This parameter is a measure of the mean wavelength content of the profile. It can be obtained from the autocorrelation function to be discussed in section 2.4.3.

Since λ_{pc} is felt to be a more relevant parameter to the surface drag problem than λ_a and since it is easier to calculate than α, we

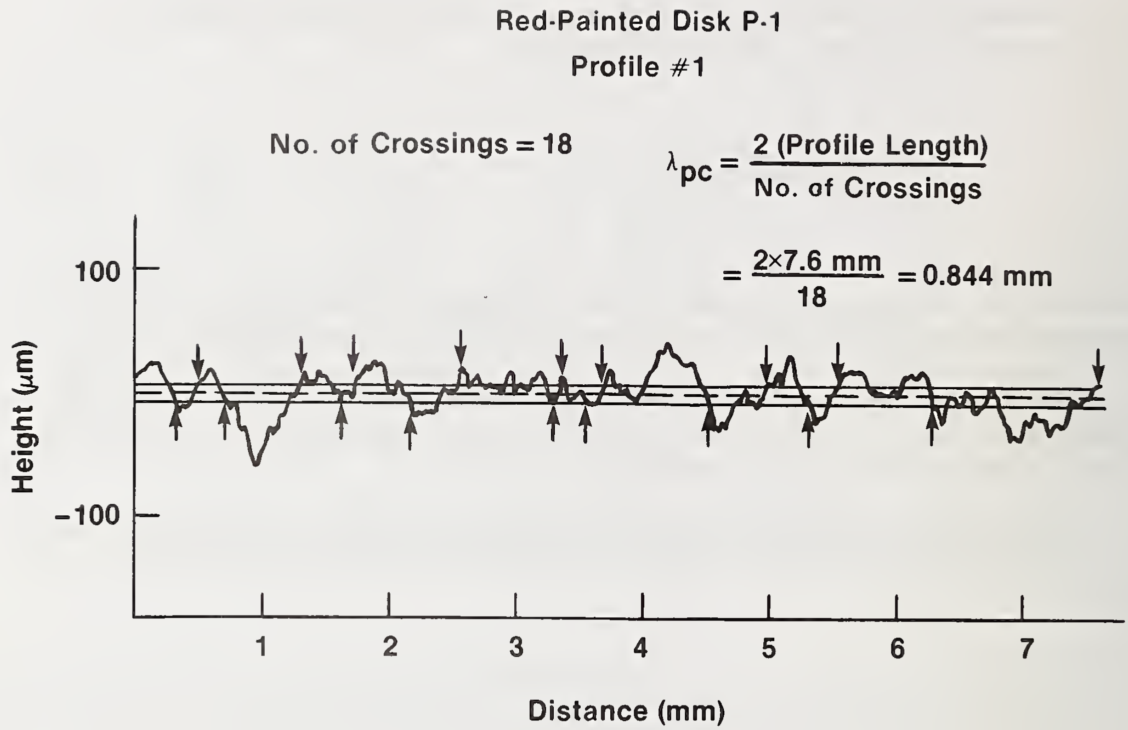

Figure 6. Typical profile trace showing a sample calculation of λ_{pc} obtained by counting the number of times that the profile is crossed by the mean band.

have used only λ_{pc} to characterize surface wavelengths in the present report.

2.4.3 Functions

In addition to the parameters discussed above, there are a number of fundamental statistical functions which characterize a surface profile in a more complete, though more complex, fashion. These functions may be used as a basis for calculating a number of the parameters already discussed.

a) Amplitude Density Function-ADF. The ADF is a probability density of surface heights. It is found by plotting a histogram of the profile points in the vertical direction as shown schematically in figure 5. R_a, R_q, and R_{max} can all be calculated from the ADF [9,15].

b) Autocorrelation Function-ACF. The ACF is one way of characterizing both the wavelength and amplitude properties of a surface. It is a quantitative measure of the similarity between a laterally shifted and an unshifted version of the profile. For a digitized profile it is given by

$$ACF\,(k\tau) = \frac{1}{N-k} \sum_{i=1}^{N-k} y_i\, y_{i+k}, \tag{7}$$

where τ is again the point-to-point spacing of the profile and $k\tau$ is the shift distance. Typical autocorrelation functions for two painted disks fabricated by DTNSRDC and autocorrelation lengths are shown in figure 7. The ACFs were all normalized to have a value of unity at a shift distance of zero. This suppresses any amplitude information in the ACF but allows a better comparison of the wavelength information in the various profiles. The autocorrelation length α is derived from the ACF and is yet another parameter for estimating spacings. It is defined as the shift distance at which the value of the ACF (or its envelope) drops to a certain fraction of the zero shift value, 0.1 and

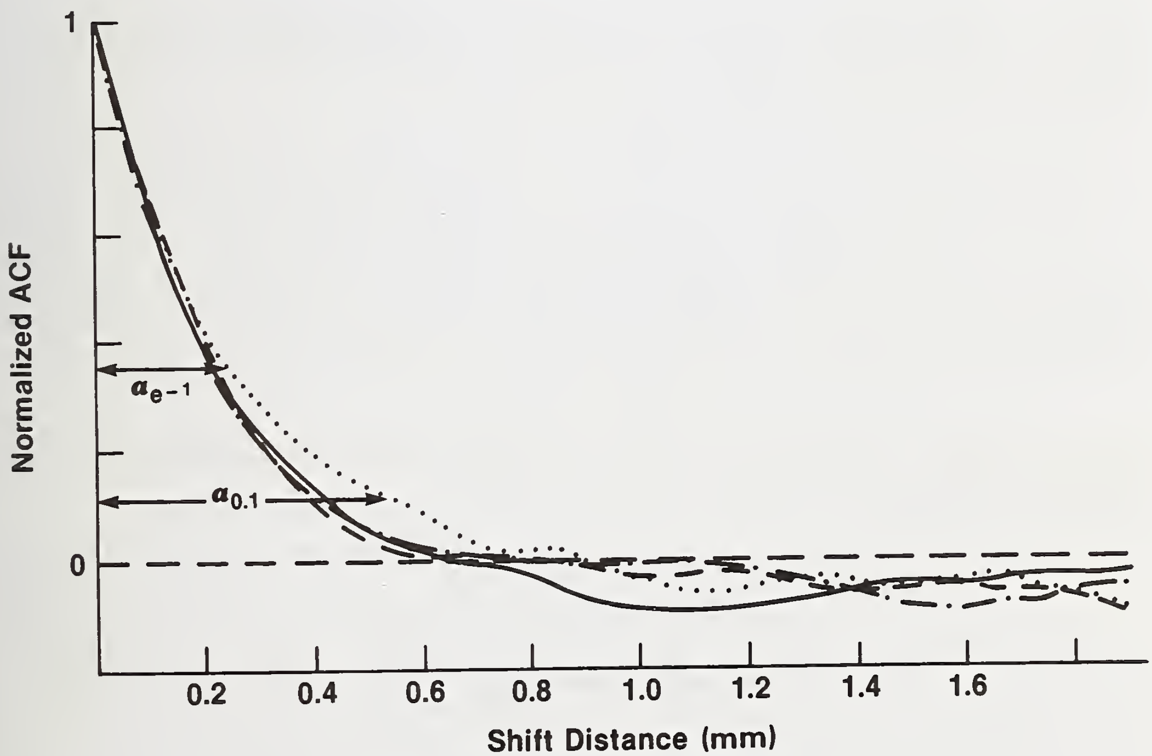

Figure 7. Normalized autocorrelation functions for 2 painted disks. ······ P-7 (new), ——— P-7 (used), -·-·-· P-15 (new), ------ P-15 (used). The autocorrelation lengths corresponding to the 0.1 point and the e^{-1} point are also shown for P-7 (new).

e^{-1} being two fractions that are commonly used (see fig. 7). Points on the profile that are separated by more than an autocorrelation length may be considered as uncorrelated, i.e., portions of the surface represented by these points were produced by separate surface forming processes. Autocorrelation lengths may range from the infinite correlation length of a perfectly periodic waveform to zero for a completely random waveform [9].

c) The Power Spectral Density-PSD. The PSD is another function for characterizing both the wavelength and amplitude properties of a surface. As discussed in section 2.1, it represents a breakdown of the surface profile y(x) into its Fourier components. It is formally given by

$$\mathrm{PSD}(f) = (1/L)\left|\int_0^L y(x)\, e^{-i2\pi fx}\, dx\right|^2, \tag{8}$$

where f is the surface spatial frequency. The PSD is also the Fourier transform of the ACF to which it is related by

$$\mathrm{PSD}(f) = 4\int_0^L \mathrm{ACF}(s)\cos 2\pi fs\pi\, ds. \tag{9}$$

Several surface parameters may be calculated from the PSD by taking moments of the form

$$M_n = \int_0^\infty f^n\, \mathrm{PSD}(f)\, df. \tag{10}$$

In particular, R_q is equal to $M_o^{1/2}$, and the rms slope is equal to $M_2^{1/2}$.

All of the above parameters are defined only in terms of two-dimensional profiles. One could define a similar set of functions in terms of three-dimensional surface maps. The question of studying three dimensional topography is explored briefly in the present work. However, it is expected that only the direction of flow is important in the drag problem so that profiles, rather than maps, are adequate to characterize the surface for drag. A study of weld beads on ships by Townsin, et al., tends to support this viewpoint [4].

Although we report the results of a large number of parameters and functions for the surfaces of rotating disks, we will confine the analysis to a few questions that we consider most important: Is R_a or R_{max} more significant in affecting drag? If neither has a predominating effect, is there an approximate multiplicative factor that one can use as a rule of thumb to relate R_{max} and R_a for ship hull surfaces? What are the relative effects of roughness and wavelength on drag, and can we express these in terms of a simple functional relationship? These questions are addressed in section 7 after a discussion of the measurement conditions and the results.

3. Experimental Details

This section describes the various rotating disks that were studied, the stylus instrument, and the surface measurement procedures.

3.1 Disks

The circular disks (fig. 8) were fabricated by DTNSRDC. They were all the same size with a diameter of about 230 mm and a thickness of about 3.2 mm, but they had varying surface textures produced by two different kinds of processes. There were eight painted steel disks (not shown) whose roughnesses were dominated by the various paint textures and nine bare, titanium alloy disks whose roughnesses were varied by varying the metal removal conditions. The disks had five holes positioned near the center for mounting in the NSRDC rotating disk apparatus. For all of the disks, the front surfaces received the same surface preparation as the back surfaces.

The eight painted disks are described in table 1. There were four different surface preparations. Disks P-1 and P-9 received a vinyl anticorrosive (AC) undercoating followed by a red antifouling (AF) overcoat; their surfaces are designated as red/vinyl. Disks P-3 and P-11 are identified as black/vinyl, disks P-5 and P-13 as red/epoxy, and disks P-7 and P-15 as black/epoxy. For each odd-numbered disk, there was an identical even-numbered disk, i.e., disks P-2 and P-10 were red/vinyl, disks P-4 and P-12 were black/vinyl and so on. The odd-numbered disks were measured for their surface finish in our laboratory, and the even-numbered disks were measured for drag at DTNSRDC.

The outer edges of the disks were also painted, but in a few spots the paint was chipped or nicked from the edges. This was not thought to have a significant effect on the drag measurements, however.

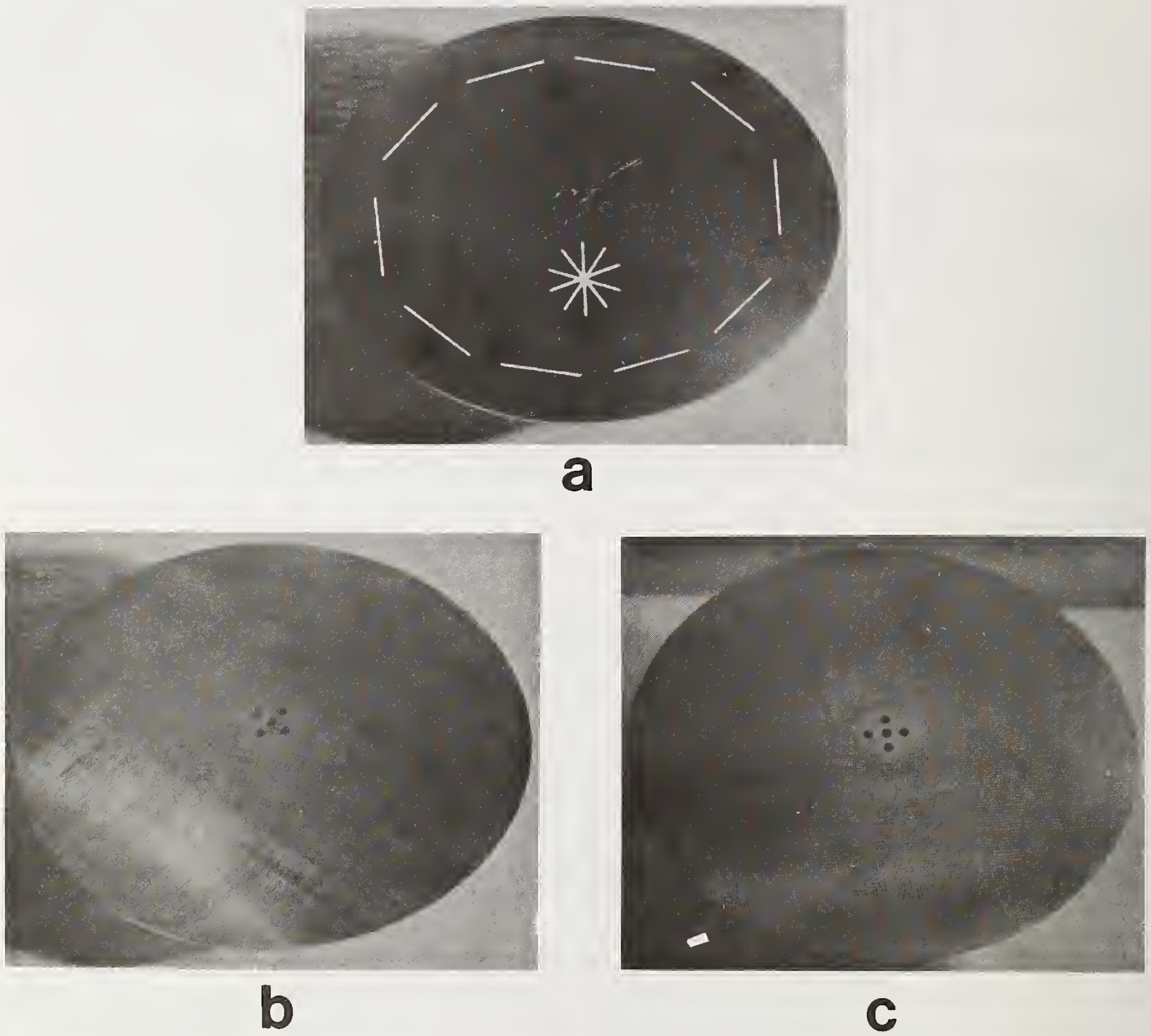

Figure 8. Photographs of the Ti alloy disks [31]. a - smooth lapped surface. Also shown in white are the tangential and directional patterns of stylus trace locations. The directional pattern shows only 5 of 11 traces.
b - close crosshatch pattern produced by end milling.
c - wide crosshatch pattern produced by end milling.

The nine titanium alloy disks are also described in table 1. Three of them are depicted in figure 8. The three smooth disks, T-1, 2, 3, were polished on a lapping machine to achieve a smooth surface, whereas disks T-4, 5, 6, 7, 8, 9 were end-milled in two directions using a V-shaped tool to produce artifically rough surfaces. The depths of cut determined the final roughnesses of the surfaces, and the resulting surfaces had highly periodic, crosshatch roughness patterns. The tool

Table 1. Descriptions of Disk Surfaces

Painted Disks

Disk I.D.	Coating Code Numbers and Descriptions
P-1	117, 119, 121 Vinyl anticorrosive (AC) undercoat followed by Red antifouling (AF) overcoat (Red/Vinyl)
P-3	117, 119, 129 Vinyl AC followed by Black AF (Black/Vinyl)
P-5	150, 151, 154, 121 Epoxy AC - Red AF (Red/Epoxy)
P-7	150, 151, 154, 129 Epoxy AC - Black AF (Black/Epoxy)
P-9	117, 119, 121 (Red/Vinyl)
P-11	117, 119, 129 (Black/Vinyl)
P-13	150, 151, 154, 121 (Red/Epoxy)
P-15	150, 151, 154, 129 (Black/Epoxy)

Ti Alloy Disks

Disk I.D.	Surface Finishing Process	Tool Feed (mm)
T-1	Lapped	-
T-2	"	-
T-3	"	-
T-4	End Milled with V-shaped cutter	0.6 (Close Crosshatch)
T-5	"	0.6 (Close Crosshatch)
T-6	"	1.4 (Wide Crosshatch)
T-7	"	1.4 (Wide Crosshatch)
T-8	"	1.3 (Wide Crosshatch)
T-9	"	0.7 (Close Crosshatch)

feeds shown in table 1 were determined by measuring the periodic grid spacing with a ruler. The 3.2-mm wide outer edges of the titanium alloy disks were smooth.

3.2 Stylus Instrumentation

Surface topography measurements were taken with a Talysurf 4[1] stylus instrument interfaced to an Interdata 7/32 minicomputer[1] [9,10]. Using an interferometrically measured step, the system was calibrated on each value of magnification employed during a measurement and a calibration constant was derived. Surface profiles were then taken with a stylus having a tip radius of ~7.5 μm and a stylus force of $\sim 5 \times 10^{-4}$ N. The stylus speed was 1.52 mm/sec. Contrary to the normal procedure, the electrical signal from the stylus transducer was not filtered. Rather, the long-wavelength cutoff and the sampling length were limited by the total trace length of 7.6 mm. It should be noted that having the cutoff limited by the trace length is not a typical mode of operation. Ordinarily the stylus instrument should have a trace length approximately equal to or greater than three cutoff lengths. In the present experiment it was important to include surface wavelengths up to several mm in the output profile rather than to filter them out.

Surface profiles of the calibrating step and the roughness area under test were stored in the minicomputer memory as 4000 digitized points after 12-bit analog-to-digital conversion. The sampling rate for the roughness profiles was 1 point/1.9 μm over the 7.6 mm traversing length. After a certain amount of data processing, the digitized numbers were written onto magnetic disks for permanent storage.

In the early stages of this work, the first measurements on the titanium alloy disks were made with an Interdata 3 computer rather than the Interdata 7/32. The surface profiles taken at that time contained 4096 points rather than 4000. In addition, the Interdata 3 did not have the capability for permanent data storage on magnetic disks.

3.3 Stylus Measurement Procedures

Two modes of measurement were used to characterize the disk surfaces. In the principal mode, profiles were taken along the tangential direction at 10 equally spaced positions around the periphery of the disk, approximately 11.5 mm from the edge as shown in figure 8. The disks were mounted on a rotary table which was positioned on the base table of the stylus instrument (fig. 9) so that the disks could be rotated to a specified angle. As a rule, 10 measurements were taken on each side of

---

[1]Certain commercial equipment, instruments, or materials are identified in this report in order to specify adequately the experimental procedure. In no case does such identification imply recommendation or endorsement by the National Bureau of Standards, nor does it imply that the material or equipment identified is necessarily the best available for the purpose.

a disk. Each of the disks was measured in this way at least once. The tangential measurements were felt to be the key ones because they sample the outer surfaces of the disks, which spin the fastest in a rotating disk apparatus and have the greatest influence on the flow. In addition, the tangential direction of the roughness profiles was close to the direction of flow of the water over the surface in the spinning disk experiment [25]. The direction of flow obviously figures most importantly in the interaction between the flow and the surface. The results of these measurements are discussed in section 4.

Tangential measurements were also used to test for surface degradation of some of the disks. The Ti alloy disks were measured for roughness soon after manufacture. They were then returned to DTNSRDC for drag testing, including various experiments relating to marine growth on the surfaces. After these tests were completed, the disks were cleaned and their surfaces were remeasured in our laboratory.

The painted disks were handled differently. The new disks were measured for roughness and were then submerged in a saline solution for extended periods in our laboratory. They were then dried and their surfaces were remeasured for roughness. The results of the surface degradation tests are discussed in section 4 along with the other tangential measurements.

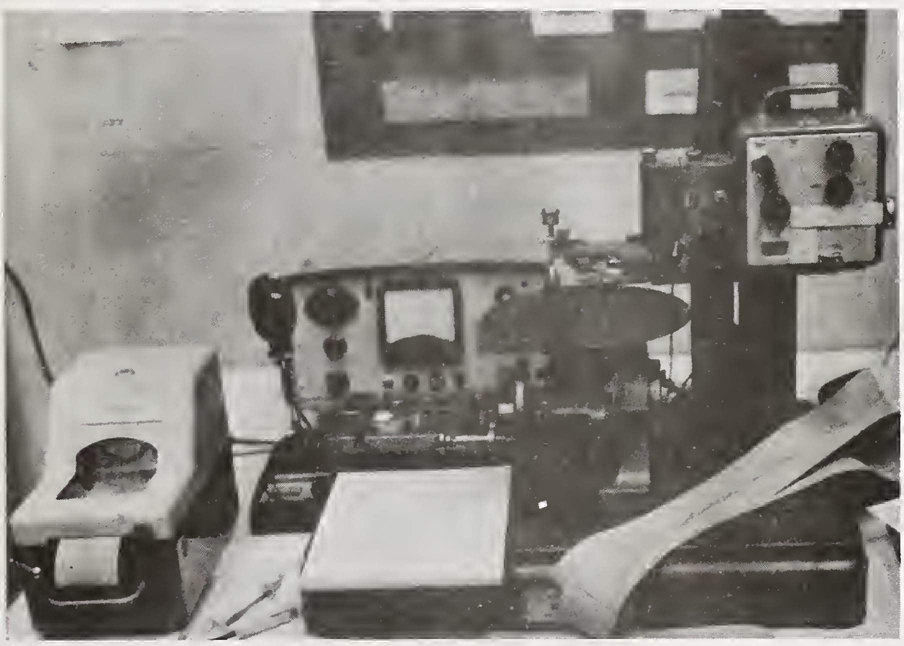

Figure 9. Photograph of a disk positioned on the rotary table and below the stylus instrument.

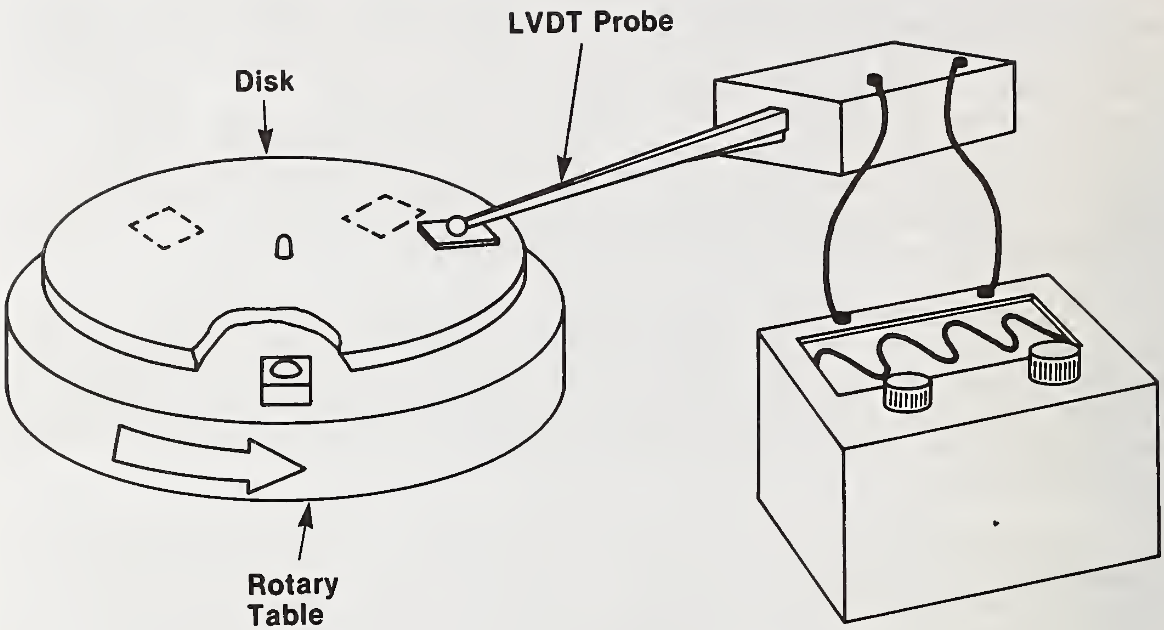

Figure 10. Schematic diagram of the waviness measuring instrument. The positions of two of the ball bearing supports are shown by the dotted parallelograms.

In the second mode, measurements were taken in 11 equally spaced directions at one position on each of seven disks as shown in figure 8. This was done to assess the possible directional properties of the surfaces. The center of the stylus trace was positioned by eye over the axis of rotation of the rotary table, and the disk was mounted on the table with its center located about 72.5 mm from the rotation axis. The results of these measurements are discussed in section 6.

For both the tangential and directional modes, stylus profiles were taken three successive times at each position. The R_a was calculated for each, and the average of the three R_a readings was recorded. Then the digitized profile data for the third traverse were written onto magnetic disk for permanent storage. The other parameters and statistical functions were calculated from the stored profiles.

3.4 Waviness Measurements

During the course of the stylus measurements, it was noted that some of the disks were obviously warped into a potato-chip shape. Since it was speculated that this warp could affect the drag properties, the structural roughness (or waviness as we shall call it) of each of the disks was measured around its entire periphery. The apparatus used for these measurements consisted of an Ultradex rotary table, a Bendix height gauge with an LVDT transducer, and a Hewlett Packard strip chart recorder. A schematic picture of the setup is shown in figure 10. The sensing element of the height gauge was cemented to a 2 cm x 1 cm x 1 mm piece of flat copper sheet which served to filter out the roughness structure from the waviness measurement. The system was calibrated on each value of magnification by traversing a gauge-block step with a height of 203 μm under the probe. Each disk was then placed on three ball-bearings located 120° apart on the table and centered by a spindle. The probe was positioned on the disk near the outer edge, and the table was set to rotating. The resulting 360° profile was output from the height gauge and recorded. The results of these measurements for peak-to-valley waviness are discussed in section 5.

4. Results of the Tangential Surface Texture Measurements

4.1 Roughness Average R_a

The R_a results for the Ti alloy disks are shown in table 2, and those for the painted disks are shown in table 3. Values for the average R_a from 10 measurements on both the front and back surfaces of the new disks are given in column 2 and the averages of each pair of readings are given in column 4. These average values represent an important roughness parameter for the disks, and they were used to characterize the disks in subsequent calculations. After immersion, sliming, and cleaning, most of the Ti alloy disks were measured again, and these results are given in columns 6 - 9 of table 2. A scan of the numbers suggests that the new and used results are quite similar. This is not surprising, since the processes of sliming and cleaning were not expected to remove any metal from the surfaces. The Ti alloy disks revealed two regimes of roughness, the lapped surfaces, T-1, 2, 3, being much smoother than the machined surfaces, T-4...9.

Similar results for the painted disks are given in table 3. It shows clearly that the pair of black/epoxy surfaces was the smoothest of the set. The black/vinyl pair was rougher, the red/epoxy pair rougher still, and the red/vinyl pair was the roughest. The red overcoat was clearly rougher than the black, but the surprise in these data was the effect of the vinyl undercoat, which gave rougher surfaces than the epoxy undercoat. Comparing the results in columns 4 and 8 suggests that soaking in saline solution did little to change the roughness values of the surfaces. The exception was the front surface of disk P-3 which, for unknown reasons, became heavily corroded with soaking. The corrosion consisted of green and rust-colored raised spots in large enough abundance that it was not feasible to make roughness measurements on the surface afterwards. The roughness of the back of this same disk was measurable, however, and its R_a value changed by only 9 percent with soaking.

The uncertainties quoted in columns 3 and 7 of both tables represent the sum of the estimated calibration uncertainty and one standard deviation of the mean for the series of readings. For a set of N numbers y_i

Table 2. Results of the R_a Measurements for Ti Alloy Disks. (The sources of the quoted uncertainty (U) are discussed in the text.)

Disk I.D.	New: Front / Back R_a µm	U µm	New: Average R_a µm	U µm	Used (After Immersion, Sliming and Cleaning): Front / Back R_a µm	U µm	Used: Average R_a µm	U µm
T-1	0.176	± 0.047	0.172	± 0.047	0.155	± 0.029	0.148	± 0.029
	0.168	± 0.027			0.140	± 0.025		
T-2[a]	0.147	0.026	0.139	0.026	0.117	0.020	0.131	0.037
					0.139	0.037		
	0.132	0.022			0.124	0.024		
					0.145	0.030		
T-3	0.176	0.039	0.165	0.039	0.133	0.025	0.136	0.025
	0.154	0.028			0.139	0.024		
T-4	9.5	1.1	10.0	1.1	--	--	--	--
	10.5	0.8						
T-5[a]	9.5	1.4	8.8	1.4	9.3	1.4	8.8	1.4
					8.2	1.4		
	8.2	1.4			9.5	1.4		
					8.4	1.4		
T-6	17.3	1.7	16.2	2.2	15.7	2.5	16.3	2.5
	15.0	2.2			16.9	1.9		
T-7	13.6	1.1	13.1	1.7	13.5	1.5	13.1	1.7
	12.7	1.7			12.8	1.7		
T-8	9.5	0.9	9.0	1.3	9.3	1.1	9.9	1.1
	8.5	1.3			10.4	1.1		
T-9	5.20	0.64	4.87	0.64	--	--	--	--
	4.53	0.53						

[a]Disks T-2 and T-5 were measured twice after being slimed and cleaned.

Table 3. Results of the R_a Measurements for the Painted Disks. (The sources of the quoted uncertainties are discussed in the text.)

Disk I.D.	New				Used (After Soaking)			
	Front Back		Average		Front Back		Average	
	R_a μm	U μm	R_a μm	U μm	R_a μm	U μm	R_a μm	U μm
P-1	14.4 ±	1.0			14.4 ±	1.1		
(Red/Vinyl)			15.1 ±	1.1			14.6 ±	1.1
	15.9	1.1			14.7	1.1		
P-3	9.0	0.9			--	--		
(Black/Vinyl)			9.0	0.9			9.8	0.7
	9.0	0.8			9.8	0.7		
P-5	14.5	1.1			14.8	1.1		
(Red/Epoxy)			13.5	1.1			13.6	1.1
	12.5	0.8			12.5	0.9		
P-7	5.15	0.64			4.60	0.60		
(Black/Epoxy)			6.28	0.98			6.29	0.75
	7.40	0.98			7.98	0.75		
P-9	14.6	1.1			12.7	1.2		
(Red/Vinyl)			16.4	1.9			14.8	1.2
	18.2	1.9			17.0	1.2		
P-11	12.1	1.2			12.4	1.1		
(Black/Vinyl)			10.5	1.2			10.6	1.1
	8.8	0.8			8.8	0.9		
P-13	12.8	1.0			13.2	1.1		
(Red/Epoxy)			13.7	1.0			13.5	1.1
	14.5	1.0			13.8	1.0		
P-15	4.79	0.46			4.92	0.47		
(Black/Epoxy)			5.66	0.74			5.63	0.61
	6.52	0.74			6.33	0.61		

with an average $\bar{y}$, one standard deviation of the mean (1 S.D.M.) was calculated by the following formula.

$$1 \text{ S.D.M.} = (1/K) \left[\frac{1}{(N)(N-1)} \sum_{i=1}^{N} (y_i - \bar{y})^2 \right]^{1/2} , \qquad (11)$$

where the factor K is a slowly varying function of the sample size N. The value of K varies between 0.797 and unity [26]; for N=10, K is equal to 0.973; for N=20, K is equal to 0.987. For most of the surfaces, the standard deviation of the mean was the larger of the two uncertainty components.

The calibration uncertainty had a systematic part and a random part and was attributed to six sources of uncertainty. The systematic part was an estimate of the differences between a value for R_a obtained with the use of the NBS stylus/computer system and a value for R_a obtained with an ideal system. These uncertainties resulted from those properties of the measurement process which are fixed prior to and during the procedure of obtaining data. The random part described the variations in the results of a measurement process during repetitions of the procedure to obtain data.

The random uncertainty was attributed to four sources: (1) the variations in the calibration constant due to the surface finish of the calibration step; (2) the variations in the calibration constant due to sampling and digitizing processes, software computations, and non-linearities in the stylus instrument transducer and in the interface hardware; (3) the variations in the measured R_a values due to the processes mentioned in (2) for a fixed calibration constant; and (4) the variation in R_a due to variations in the average slope of the unfiltered profile. Sources of the systematic uncertainty were: (5) uncertainty in the height of the calibrating step obtained from interferometric measurements and (6) uncertainty in the stylus tip radius.

The uncertainty of each average result in tables 2 and 3 was simply taken as the larger of the pair of uncertainties for the front and back surfaces.

A number of comparison tests was made with the data of tables 2 and 3 to test for systematic effects of several factors on the surface roughness. First, the differences between the R_a values for new and used disks were calculated to determine whether the surface changed significantly with use. Second, the differences between R_a values for the front and back surfaces of the new disks were calculated as indicators of how consistent the machining or painting processes were. Finally, the differences in R_a between the members of the various pairs of painted disks were calculated as further indicators of the consistency of

Table 4. Comparison Tests: Average Absolute R_a differences between the Various Sets of Disks

	Front-Back μm	New - Used μm	Differences Within Pairs Of Similar Surfaces μm
Ti Alloy 1-3	0.015 ± 0.045	0.020 ± 0.049	--
Ti Alloy 4-9	1.2 ± 1.8	0.25 ± 2.4	--
Painted	2.0 ± 1.4	0.4 ± 1.5	0.9 ± 1.6

the painting process. The calculations were done by taking absolute differences between corresponding members of a pair and then calculating average values for all of the pairs in a set. The results are shown in table 4,and an example of one calculation is as follows. The absolute differences between the front and back R_a measurements for the new lapped, Ti alloy disks (T-1, 2, 3) were 0.008, 0.015, and 0.022 μm. The average absolute difference of 0.015 μm is shown in table 4. The uncertainty of this value was estimated by taking the quadratic sum of the uncertainties in each pair and averaging over all the pairs in a group. For example, the estimated uncertainty in taking the T-1 front-back difference was $[(0.047)^2 + (0.027)^2]^{1/2} = 0.054$ μm, and the average uncertainty for disks T-1, 2, 3 was $(.054 + 0.034 + 0.048)/3 = 0.045$ μm.

Since almost all of the average differences are smaller than the estimated uncertainties, it seems likely that the machining and lapping processes were fairly consistent from front to back, the painting processes were fairly consistent from one disk to the next, and the disk surfaces did not change significantly with use. The above conclusions were further supported by standard analysis-of-variance tests [27]. The average difference of 2.0 ± 1.4 μm between R_a values for the front and back surfaces of the painted disks suggests that there may have been some inconsistencies in the paint application between front and back surfaces, but the difference does not seem to be very large.

Table 5. Results for the peak-to-valley roughness R_{max} for all disks. (The sources of uncertainty are discussed in the text.)

Disk I.D.	New µm	Used µm	Average µm
T-1	-	1.83 ± 0.23	
T-2[a]	-	1.36 ± 0.14 1.65 ± 0.19	1.51 ± 0.17
T-3	-	1.47 ± 0.16	
T-4	40.2 ± 2.8		
T-5[a]	-	37.6 ± 3.4 37.2 ± 3.3	37.4 ± 3.4
T-6	-	83.7 ± 8.5	
T-7	-	68.2 ± 5.5	
T-8	-	56.4 ± 4.1	
T-9	23.4 ± 1.8		
P-1	103.3 ± 6.7	96.5 ± 6.5	
P-3	60.5 ± 4.6	60.8 ± 4.5	
P-5	90.6 ± 6.9	96.7 ± 6.4	
P-7	43.4 ± 4.8	40.7 ± 4.3	
P-9	107.3 ± 8.0	100.7 ± 8.1	
P-11	69.0 ± 7.5	70.2 ± 6.7	
P-13	93.7 ± 6.2	93.1 ± 6.0	
P-15	40.4 ± 3.9	40.2 ± 3.0	

[a]Disks T-2 and T-5 were measured on two occasions after they were slimed and cleaned.

4.2 Peak-to-Valley Roughness - R_{max}

The results for the peak-to-valley roughness R_{max} are given in table 5. Once again, the differences between the new and used painted disks seem insignificant. The new Ti-alloy disks were measured before the data storage system was in operation and before the system possessed the capability of calculating R_{max}. Moreover, disks T-4 and T-9 were not available for surface measurement after they were slimed and cleaned. Therefore, in order to obtain at least one full set of R_{max} results,we calculated values for R_{max} of T-4 and T-9 by hand using the original profile traces obtained when the disks were new. From the R_a consistency checks of table 4, we did not expect significant differences in the R_{max} values between the new and used disks, so it was not necessary to do the hand calculations for all the new disks.

If the ratio R_{max}/R_a were fairly constant,it would be possible to propose an approximate rule-of-thumb for these surfaces to convert R_{max} results to R_a and vice versa. Values of R_{max}/R_a are shown in table 6. The average values can be used as approximate conversion factors for each of the three types of surfaces. A truly random surface

Table 6. R_{max}/R_a Ratios. (The uncertainty of each average value is the standard deviation of the set of measurements.)

	Disk I. D.	R_{max}/R_a	Average
Lapped	T-1	10.64	
Ti Alloy	T-2	10.86	10 ± 1
	T-3	8.91	
Machined	T-4	4.02	
Ti Alloy	T-5	4.25	
	T-6	5.17	
	T-7	5.21	5.0 ± 0.8
	T-8	6.27	
	T-9	4.80	
Painted	P-1	6.84	
	P-3	6.72	
	P-5	6.71	
	P-7	6.91	
	P-9	6.54	6.8 ± 0.2
	P-11	6.57	
	P-13	6.84	
	P-15	7.14	

with a Gaussian ADF would be expected to have a high R_{max}/R_a ratio of ~10; whereas, a truly periodic surface would be expected to have a R_{max}/R_a ratio of only 3-4 or so. These considerations agree with the results of table 6. The surfaces produced by lapping, a fairly random process, have large R_{max}/R_a ratios, whereas the surfaces produced by the deterministic milling process have the smallest R_{max}/R_a ratio. These differences are also revealed by the surface profiles shown in figures 1, 6, and 11. There is clearly a difference between the lapped surface profile of disk T-2 with its jagged peaks occurring at different heights and the machined profile of disk T-8 with its periodic flat peaks.

The estimates of uncertainty in R_{max} are derived from the same sources as those for R_a. Since we had already tested the differences between the front and back surfaces with the R_a results, no attempt was made to compare the R_{max} measurements of front and back surfaces. Consequently, the quoted values of R_{max} are simply the averages of all 20 measurements on each disk surface. The random component of the uncertainty was the estimated standard deviation of the mean (eq. 11) of each set of 20 measurements.

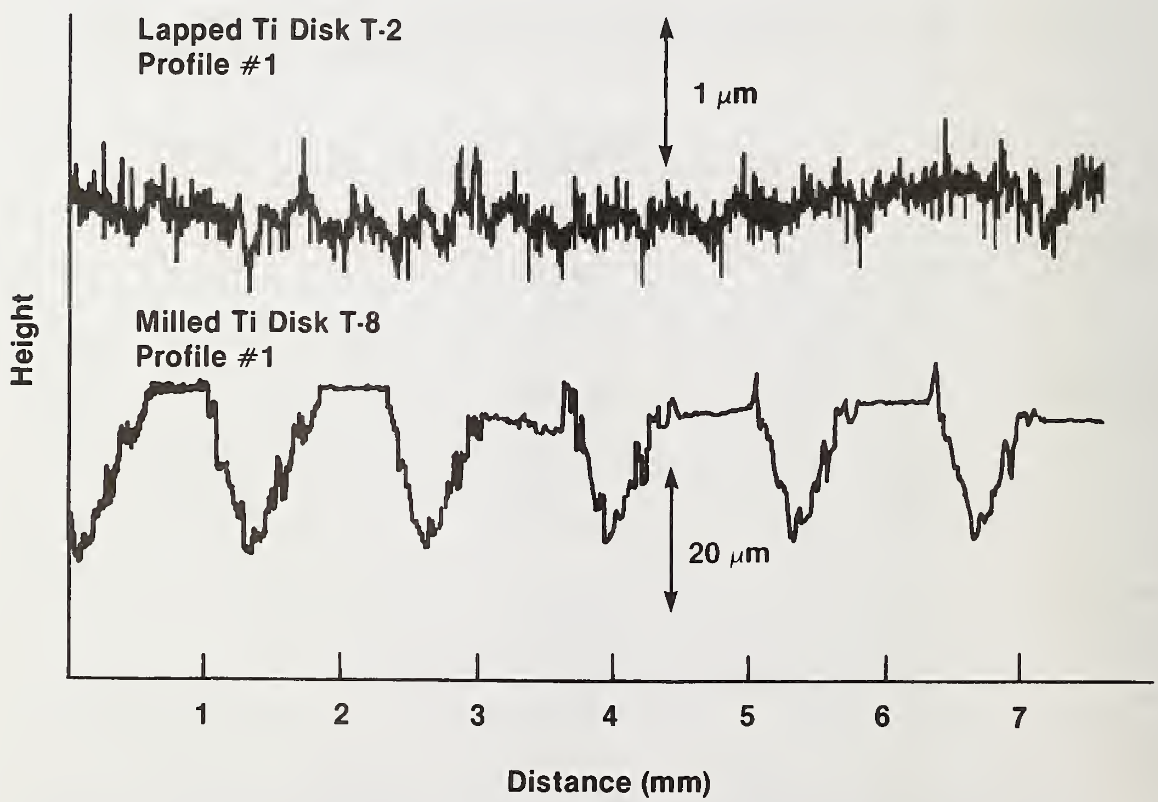

Figure 11. Typical surface profiles of two Ti alloy disks.

4.3 Peak-Count Wavelength - λ_{pc}

The results for λ_{pc} are given in table 7. The lapped Ti alloy surfaces have the finest spacings ($\lambda_{pc} \sim 0.1$ mm) whereas the machined surfaces have the widest spacings, resulting from the tool feed of ~1 mm . The uncertainties of these values represent the sum of the

Table 7. λ_{pc} Results for All Disks.

Disk I. D.	New mm	Used mm	
T-1	-	0.139 ± 0.027	
T-2	-	0.088 ± 0.027 0.115 ± 0.025	0.102±0.027
T-3	-	0.090 ± 0.012	
T-4	0.92 ± 0.14	-	
T-5	-	1.16 ± 0.18 1.18 ± 0.19	1.17 ±0.19
T-6	-	1.88 ± 0.27	
T-7	-	1.61 ± 0.15	
T-8	-	2.10 ± 0.30	
T-9	0.899 ± 0.080	-	
P-1	0.884 ± 0.082	0.825 ± 0.075	
P-3	1.01 ± 0.14	1.00 ± 0.16	
P-5	0.633 ± 0.061	0.716 ± 0.068	
P-7	1.22 ± 0.40	0.87 ± 0.11	
P-9	0.96 ± 0.10	0.796 ± 0.070	
P-11	1.14 ± 0.15	0.96 ± 0.10	
P-13	0.651 ± 0.080	0.709 ± 0.085	
P-15	0.745 ± 0.091	0.769 ± 0.083	

estimated calibration uncertainty and the estimated 1 S.D.M. The calibration uncertainty is simply equal to 3.5 percent of the λ_{pc} value, and it arises from the uncertainties in measuring the wavelength of the periodic roughness artifact used to calibrate the horizontal travel on the stylus. The sample random uncertainty is the larger of the two components. In the case of disks T-6 and P-7, the large uncertainty was due almost entirely to the sample random uncertainty.

4.4 Other Parameters

The average results for the rms roughness R_q, average slope S_a, and average wavelength λ_a are shown in table 8. These parameters were not used in any subsequent calculations to characterize the disk properties. The R_q parameter measures essentially the same surface property as R_a and yields very little new information. S_a and λ_a are sensitive to the finer surface texture, whereas we expect that the surface drag of the disks should depend more on the larger surface features with wavelengths of ~1 mm.

4.5 Statistical Functions

Some of the statistical functions calculated from the profile measurements are shown in figures 7 and 12-14. Each function is an aver-

Table 8. Results for Additional Surface Texture Parameters

	R_q μm	S_a	λ_a mm
T-1	0.21	0.020	0.047
T-2	0.17	0.020	0.041
T-3	0.17	0.021	0.041
T-4	--	--	--
T-5	10.1	0.10	0.58
T-6	19.9	0.14	0.78
T-7	15.7	0.14	0.60
T-8	12.3	0.12	0.55
T-9	--	--	--
P-1	18.9	0.28	0.34
P-3	11.4	0.19	0.30
P-5	16.8	0.31	0.28
P-7	8.0	0.16	0.24
P-9	20.6	0.28	0.36
P-11	13.0	0.22	0.31
P-13	17.2	0.31	0.27
P-15	7.1	0.17	0.21

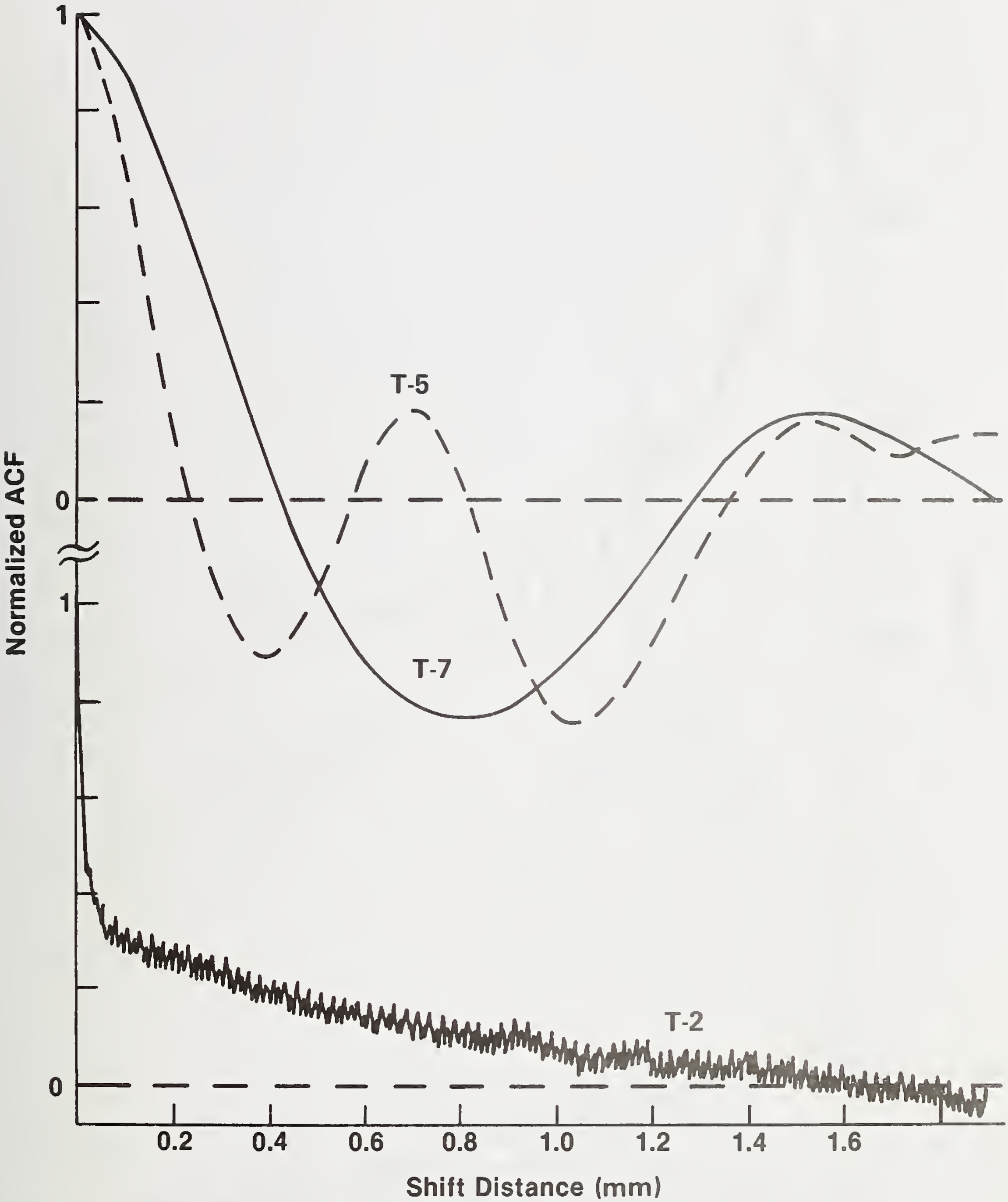

Figure 12. Normalized ACFs for Ti alloy surfaces. The curve for T-2 has been displaced downward from the other two for clarity.

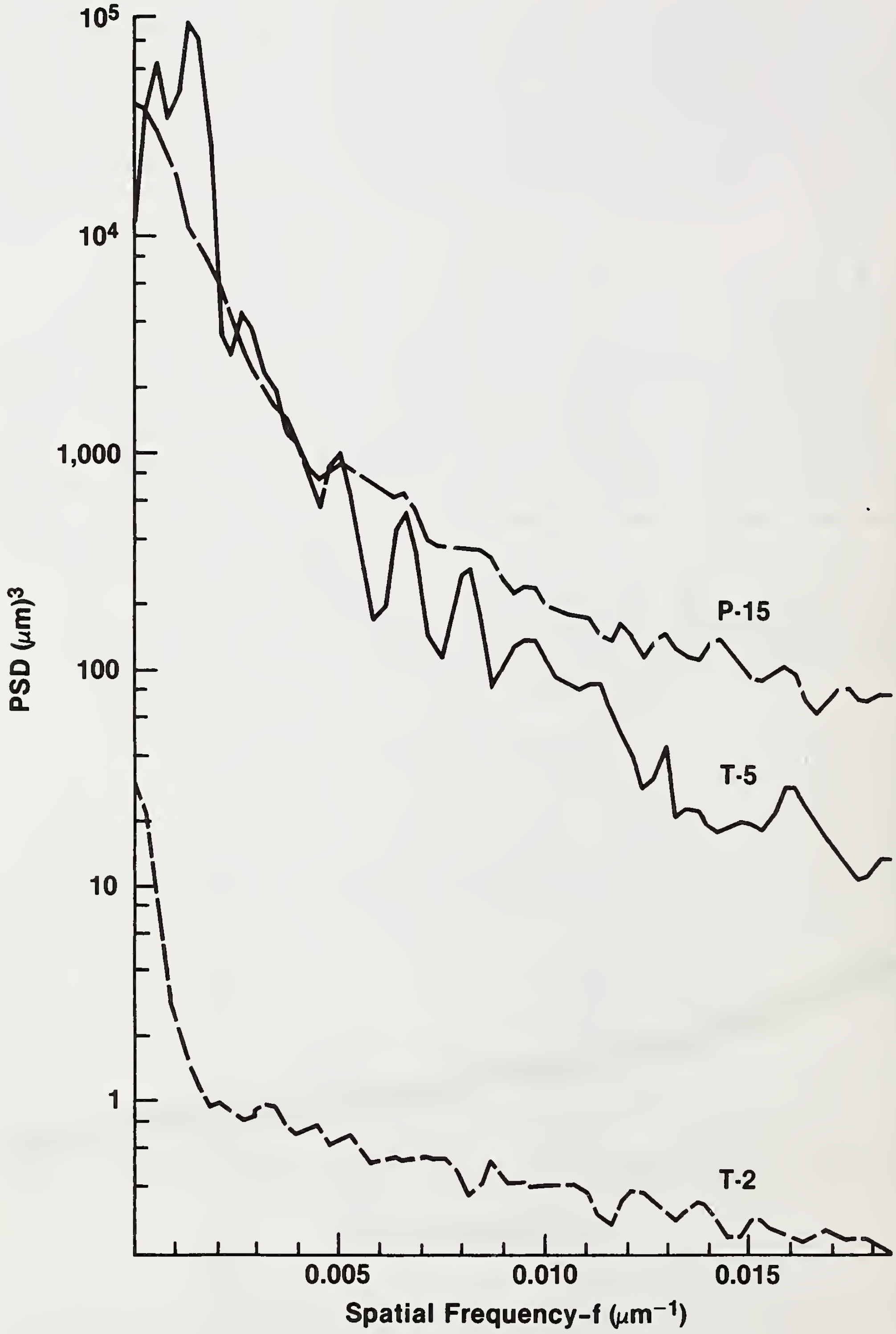

Figure 13. PSDs for three disks.

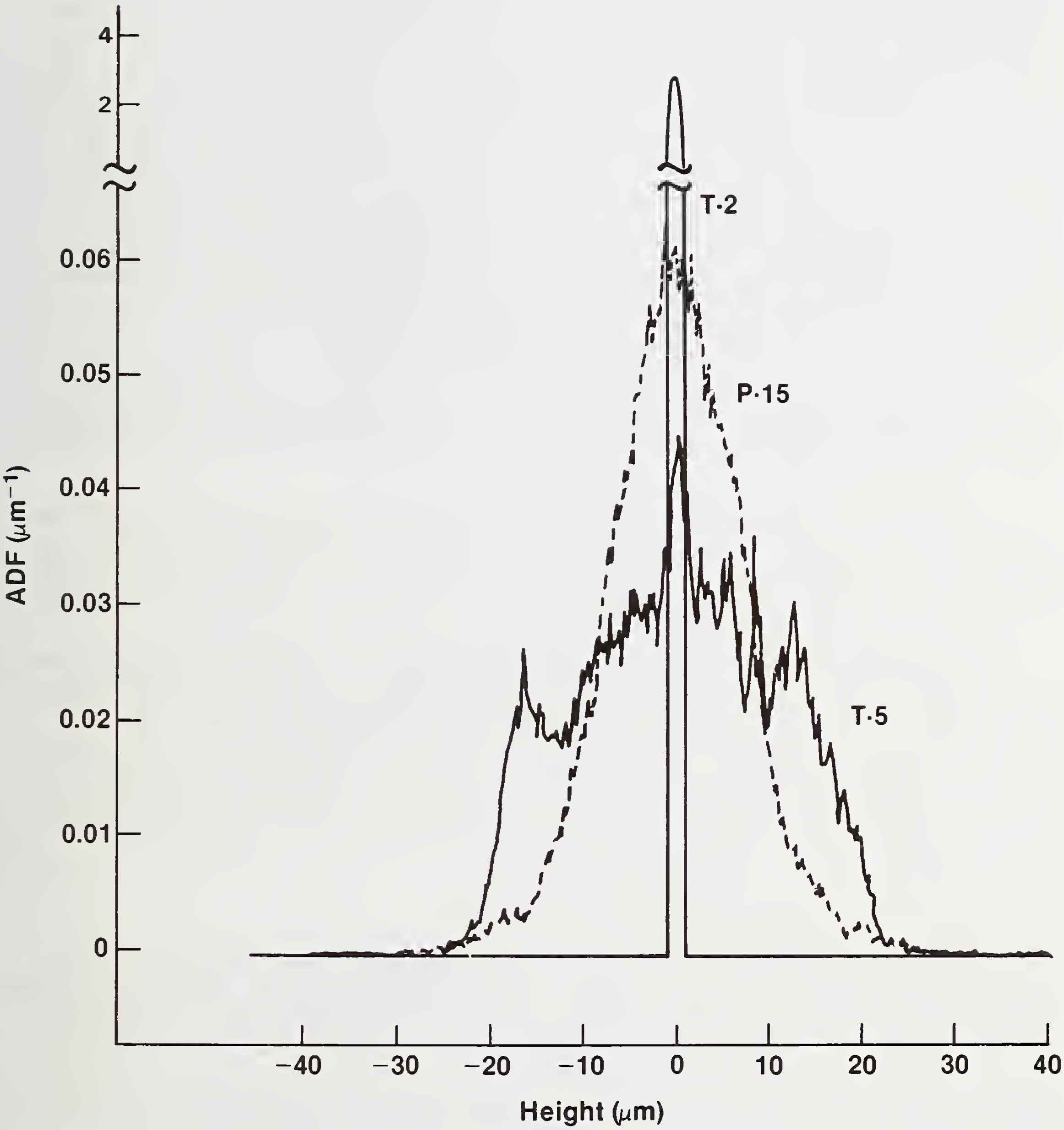

Figure 14. ADFs for the same three disks as in figure 13.

age of the functions calculated from the 20 surface profiles taken on the disk.

The ACFs for disk P-7 and P-15 (fig. 7) show a decay that is fairly close to exponential, an observation which suggests that these painted disks have a fairly random structure. Disks T-5,7 (fig. 12) have ACFs with a very strong periodic structure, as expected. The curve for T-2 exhibits two decay rates, thus indicating two orders of surface structure. The fine microroughness structure yields the sharply decaying peak with a width of ~50 μm, but there is also a longer wavelength waviness structure in the surface profiles which yield the gently sloping part of the ACF. Superimposed on both of these features is a fine periodicity with a wavelength of ~12 μm. This latter feature is not due to any real surface structure, but rather to a component of noise in the instrument which crops up at the very high magnifications required to measure smooth surfaces like T-2. This noise component does not contribute significantly to errors in the R_a or R_{max} measurements.

In figure 7, disks P-7 and P-15 are twins, and as expected, their ACFs are quite similar. In addition, it is seen that their ACFs changed very little with use.

The PSDs of figure 13 reveal both amplitude and wavelength information. The figure is plotted on a semilog scale spanning five orders of magnitude to compare the smooth and rough surfaces. The periodic nature of T-5 is once again revealed by the set of discrete peaks in its PSD.

The ADFs of figure 14 are also enlightening. P-15 is a fairly random surface so its ADF is bell-shaped and resembles a Gaussian function. T-5, however, is periodic so its ADF has two peaks at heights of ~±18 μm in addition to the one at zero. T-2 is so smooth that its surface structures span only a very narrow range of heights; therefore, its ADF looks like a spike when plotted on the same scale as the other two.

5. Structural Roughness (Waviness) Results

Subsequent to the drag and the roughness measurements, the structural roughness of the disks was studied to measure the long-wavelength surface structure, not accounted for in the roughness results, and, in particular, to test whether the obvious waviness of some of the disks affected drag. Since the waviness could vary significantly from one disk to the next, it was necessary to measure the very disks that had been studied in the drag experiments. Consequently, waviness profiles were made on six of the even-numbered, painted disks, in addition to their odd-numbered twins, and the titanium disks as well.

The measurement procedure was described in section 3.4. Some of the more interesting waviness profiles are shown in figure 15, and the results for the peak-to-valley waviness W_{max} are given in table 9. As expected, W_{max} is many times greater than the peak-to-valley roughness R_{max}.

It should be noted that the profiles, and hence W_{max}, depend somewhat on the leveling procedure described in section 3.4. When a disk is highly warped, one can rotate the disk with respect to the ball bearings on which it lies and get different profiles, and hence slightly different results for W_{max}. Disk P-9 was lying level on the ball bearings. Hence the profile in figure 15 shows two peaks, which correspond to the two flaps of the potato-chip shape. These are separated by about 180°, or ~360 mm around the circumference, and they have approximately equal height. On the other hand, the profile for disk T-1 suggests that T-1 was probably laid upside down with one flap of the potato chip pointing down and the other flap lying level. Hence, the peaks are not of equal height. Although it is possible to develop a suitable procedure to define the leveling component in the waviness profile and correct for it, this was not considered necessary in the present study. The results are meant to be only an approximate indicator of the waviness of the disks, say to within a factor of two. As we shall see in section 7, the results are accurate enough to suggest that the waviness did not affect drag. In this respect, the profiles for disks T-1 and T-2 (fig. 15) and the corresponding waviness values (table 9) proved particularly interesting. These disks had highly polished surfaces with similar roughness values, but the waviness differed by almost an order of magnitude.

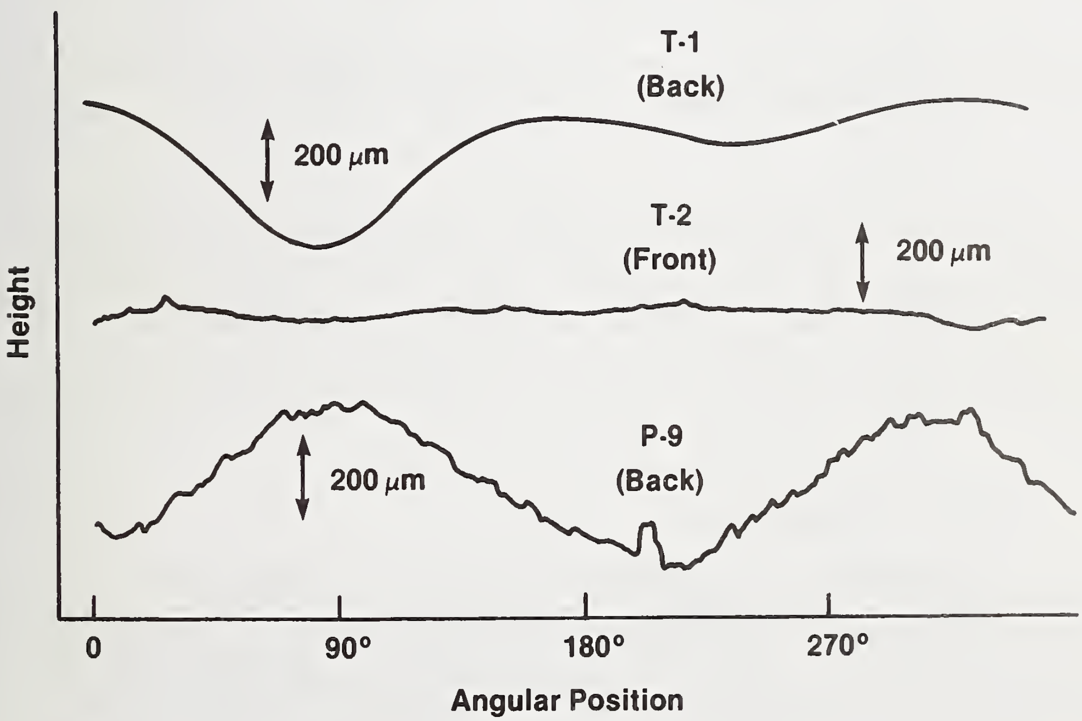

Figure 15. Waviness profiles for three disks. A complete rotation of 360° corresponds to 718 mm around the periphery of the disks.

Table 9. Results for the Peak-to-Valley Waviness W_{max} of the Test Disks.

Disk I. D.	Front mm	Back mm		Front mm	Back mm
T-1	0.47	0.42		-	-
T-2	0.05	0.07		-	-
T-3	0.34	0.36		-	-
T-4	0.45	0.41		-	-
T-5	0.46	0.50		-	-
T-6	0.20	0.20		-	-
T-7[a]	0.11	0.12		-	-
T-8	0.33	0.26		-	-
T-9	0.24	0.34		-	-
P-1	0.88	0.80	P-2	1.1	>1.0
P-3	0.82	0.99	P-4	-	-
P-5	0.94	0.89	P-6	1.0	1.0
				0.93	0.87
P-7	0.86	0.91	P-8	-	-
P-9	0.59	0.48	P-10	1.0	1.0
P-11	0.71	0.93	P-12	1.1	1.1
P-13	0.69	0.66	P-14	1.1	1.1
P-15	0.91	0.94	P-16	0.99	1.0

[a]This disk was not leveled by the three ball approach discussed in the text. It was measured while lying flat on the rotary table.

The waviness measurements were made several months after the drag experiments. The warp of the disks could have changed in the interim, depending on how they were cared for. Thus, a more definitive experiment on waviness would involve waviness measurements taken before and after the corresponding drag measurements. This consideration does not seem important, however, since no correlation between the waviness and drag results was observed.

6. Directional Measurements

The original reason for taking the directional measurements was to assess whether the overall three-dimensional surface structure affects the hydrodynamic flow over surfaces. After the project was begun, we realized that the direction of flow was the predominant one in the drag problem. This view is evident in the work of Townsin, et al., [4] in their studies of the effects of weld beads and plate edges on drag and in the work of Allan and Cutland [28]. A second factor that reduced the importance of the directional measurements was the difficulty of studying directional effects on drag in a spinning disk apparatus. Such studies would involve fabricating spiral roughness patterns on the disks, certainly an expensive operation, and it is not clear that any important new information would be gained in the effort.

Therefore, the measurements described in this section represent a preliminary attempt to assess the sensitivity of our methods to the directional properties of the surface topography, in case it becomes necessary to measure these properties later on. Previous work along these lines was done by Kubo and Peklenik [29] and Tanimura, et al. [30]. As described in section 3 and shown in figure 8, measurements were taken at one position in 11 directions ranging from 0° to 180°, and therefore spaced by 18°. The lapped disk T-3, the machined disks T-5 and T-8, and the painted disks P-1, P-3, P-9, and P-11 were measured in this way. From the data, we plotted polar maps showing the variation of R_a and the e^{-1} autocorrelation length with direction. Since the results should be insensitive to a reversal of the stylus tracing direction, the values at each angle θ were also plotted at θ+180°. In addition, the angles 0° and 180° represent the same direction, so the results at these two angles were averaged and the average value plotted for both the 0° and

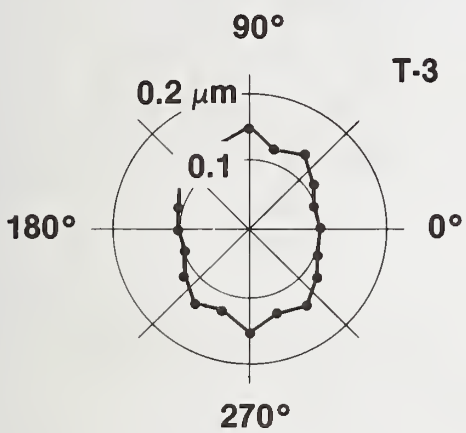

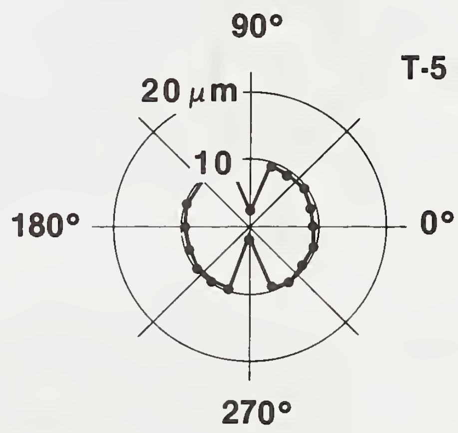

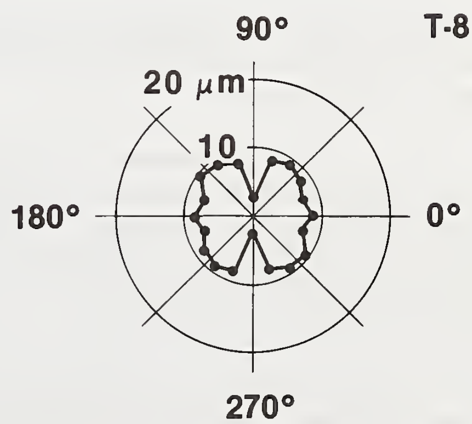

Figure 16.
R_a maps for three Ti alloy disks. These maps are based on measurements taken between 0° and 180° as indicated by the heavy dots. The R_a result at each angle θ was also plotted at θ+180°. The curves are therefore symmetric with respect to rotation of 180°.

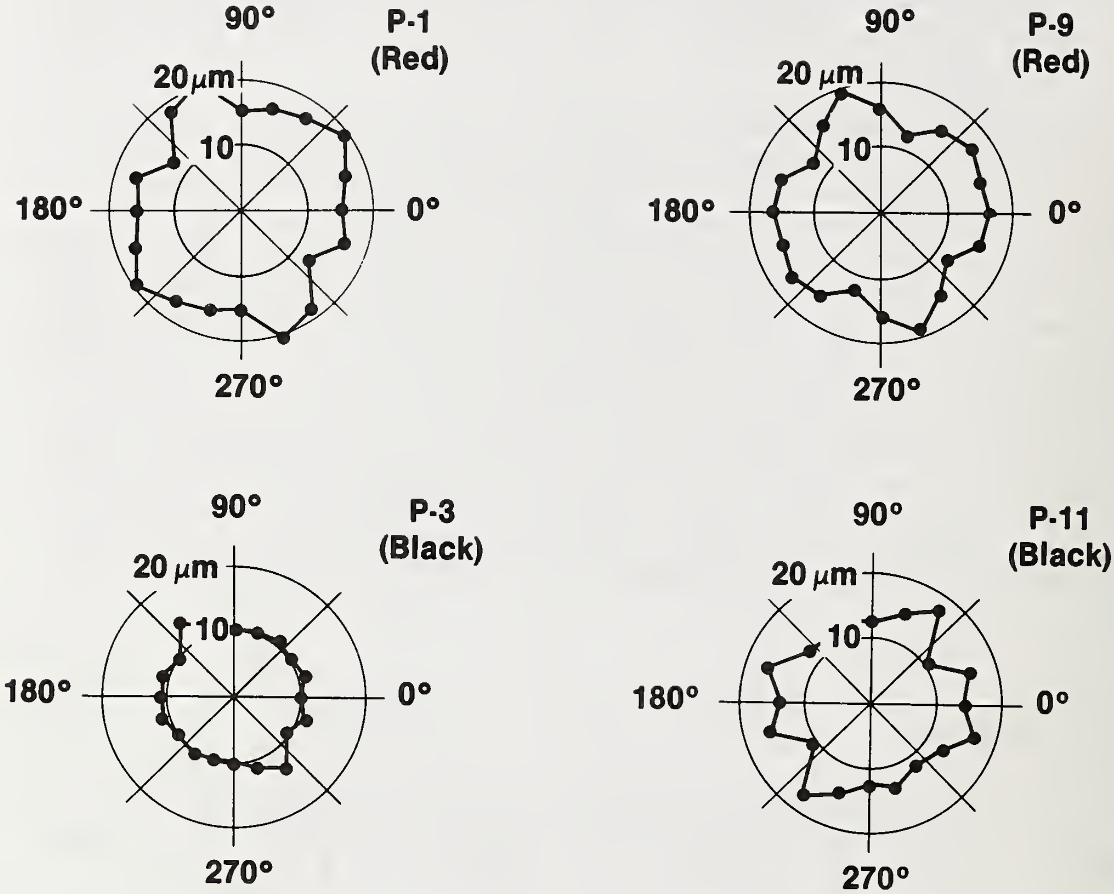

Figure 17: R_a maps for four painted disks. The results are based on measurements taken between 0° and 180° and the curves are symmetric with respect to a rotation of 180°.

180° directions. As shown in the past [29-30], the autocorrelation map seems to be more sensitive than the R_a map to directional effects in the surface structure.

The R_a maps are shown in figures 16 and 17. The R_a map for the lapped specimen T-3 (fig. 16) seems to show the anisotropies of the surface. As shown in figure 8, the lapping process left a faint lay pattern on the surface. Apparently on T-3, the lay direction was close to the 0° - 180° direction, since R_a was smallest in that direction and greatest at θ=90°.

The R_a maps for the machined surfaces, T-5 and T-8, (fig. 16) reveal striking anisotropies, as expected for these highly deterministic surfaces. The R_a values for θ=90° are much smaller than those for the other

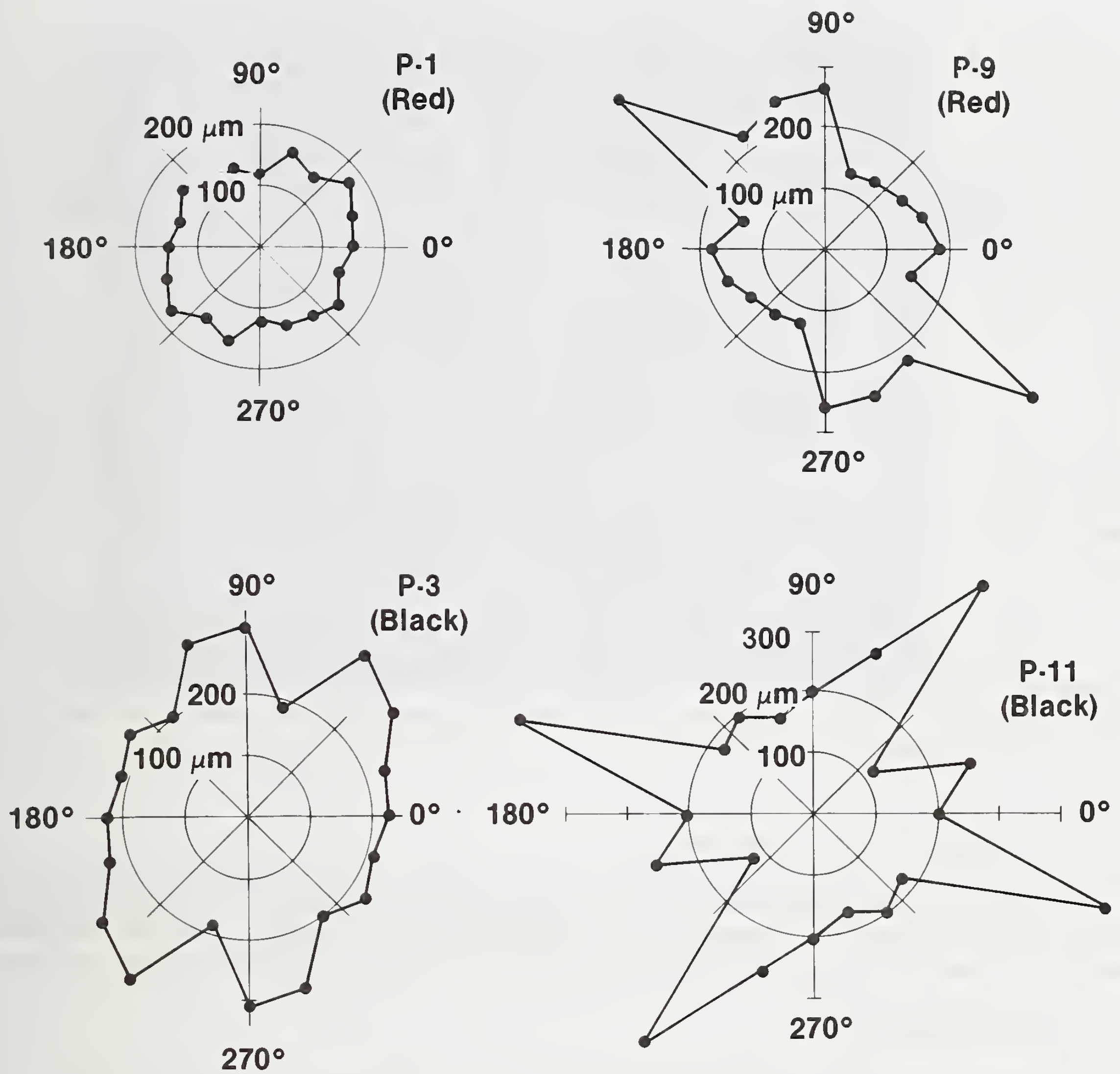

Figure 18: e^{-1} Autocorrelation length maps for the same four painted disks as figure 17. The curves are symmetric with respect to a rotation of 180°.

directions, because in that direction the stylus was tracing along one of the grooves and completely missed the surface peaks. Indeed, the character of the maps should depend on the position of the center of the stylus traces relative to the peaks of the surface. If the center were positioned on one of the peaks, then the R_a map should be fairly isotropic. If the center were positioned at the intersection of two grooves, the map would show four clefts, separated by 90°, rather than the two shown here. By contast the painted disks appear to be more isotropic. The R_a maps (fig. 17) show much smaller variations from one direction to the next.

The e^{-1} autocorrelation maps are plotted in figure 18. These are similar to autocorrelation maps discussed by Kubo and Peklenik [29] and Tanimura, et al. [30]. The lag distance at which the autocorrelation function is equal to e^{-1} (0.3769) is plotted versus direction. Results are shown only for the painted disks. The ACF results for the Ti alloy disks were obtained by the older computer system. On that system, the ACF calculation did not include a calculation of the zero line, thereby making it impossible to calculate the e^{-1} length for the titanium disk directional data. It is clear from figure 18, however, that the e^{-1} autocorrelation length plots are much more sensitive to anisotropies than the R_a plots. Slight changes in the surface topography in certain directions cause striking lobes in the e^{-1} maps. It should be noted that we are only discussing the local surface topography near one point of the surface. The painted surfaces seem to be quite isotropic on the large scale, and averaging data over several positions should reduce the anisotropies considerably. However, if real anisotropies exist on surfaces, the e^{-1} autocorrelation maps should be much more sensitive to them than the R_a maps.

In conclusion, then, the overall three-dimensional structure should not be as important in the drag problem as the two-dimensional structure measured along the direction of flow. If three-dimensional structure were important, the e^{-1} autocorrelation plot would be a sensitive way to search for directional properties.

7. Relating Drag and Roughness

In this section we show that a significant correlation exists between different measures of roughness and the drag of the disks, and we discuss empirical models to predict the drag behavior from roughness measurements.

7.1 Drag Measurements

The drag measurements were made by Belt and Smith [31,32], using the DTNSRDC rotating disk apparatus shown in figure 19. This instrument measures the torque (2τ) required to spin a fully immersed disk as a function of the angular rotational speed ω (expressed in radians/sec). The symbol τ itself is used to represent the torque on a spinning disk that is wetted on only one side. Each disk was mounted on the end of a vertical shaft in the housing shown, which was then filled with water. Power was supplied to the shaft by the motor whose rotational speed could be varied between 800 and 2200 rpm, and both the torque and the rotational speed were measured simultaneously [31]. At these speeds, the flow over the outer edges of the disks was in the turbulent regime. The torque measurements had a repeatability of about 0.8 percent. After undergoing suitable experimental corrections, the torque data were converted to dimensionless drag coefficients C_m, and the rotational speeds ω were converted to Reynold's numbers. The Reynold's number Re, also a

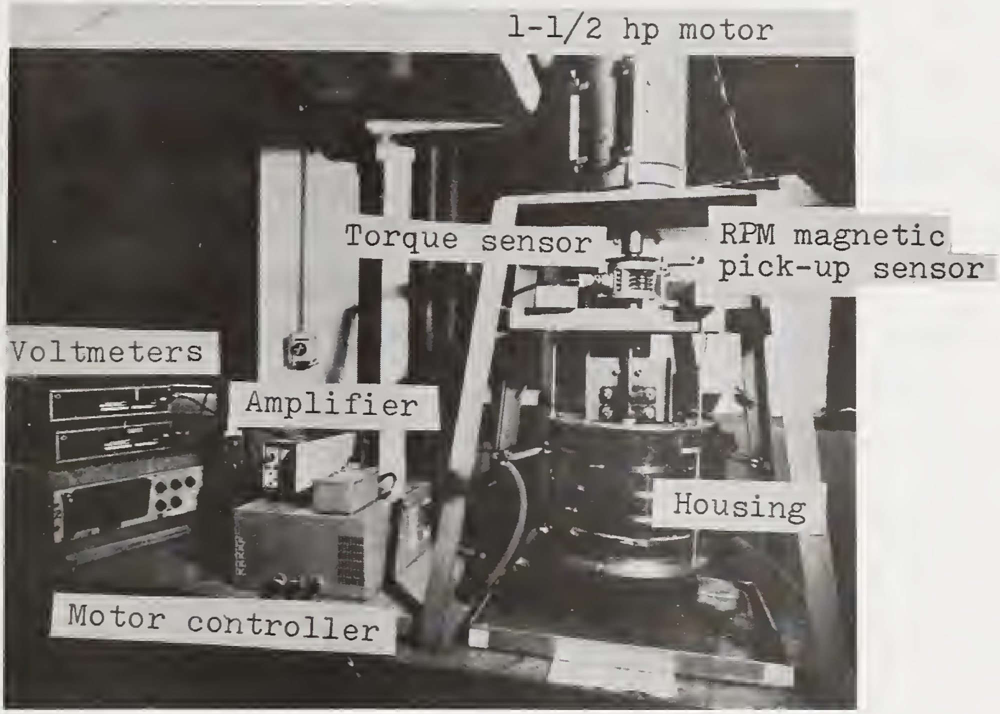

Figure 19. Photograph of the rotating disk apparatus [31].

dimensionless parameter, is the most fundamental parameter for characterizing fluid flow. For rotating disks, Re is given by [33]

$$Re = \omega r^2/\nu \ , \tag{12}$$

where r is the disk radius (~114 mm) and ν is the kinematic viscosity, defined as

$$\nu = \eta/\rho \ , \tag{13}$$

where η is the viscosity and ρ the density of the fluid (water in this case). The drag coefficients C_m were expressed in terms of the measured torque (2τ) by

Table 10. Results for the Drag Coefficient C_m interpolated to a Reynold's Number of $1.5X10^6$.[a]

Disk	C_m
T-1	$6.70X10^{-3}$
T-2	6.65
T-3	6.60
T-4	7.82
T-5	7.34
T-6	7.94
T-7	7.48
T-8	7.16
T-9	7.08
P-2	8.65
P-4	7.55
P-6	8.55
P-8	7.20
P-10	8.75
P-12	7.30
P-14	8.50
P-16	7.30

[a]Data supplied by G. Belt, N. A. Smith, and D. R. Laster [31,32]

$$C_m = \frac{2\tau}{1/2\rho\omega^2 r^5} , \tag{14}$$

The results for the drag coefficient C_m were then interpolated to the same Reynold's number of 1.5×10^6, which corresponds to a rotational rate of ~1000 rpm, to facilitate the comparison with roughness. In this connection it is important to restate that, while all of the titanium alloy disks underwent both drag and roughness measurements, the painted disks required the comparison of drag results measured for the even-numbered disks with the roughness results measured for their odd-numbered twins.

The results for C_m are shown in table 10 and are plotted as a function of average roughness R_a in figure 20. In spite of the deviations, the data of figure 20 show a strong correlation between the drag coefficient C_m and the average roughness R_a. The drag coefficient of the roughest disk is 30 percent greater than those of the smoothest disks, and this dependence of C_m on R_a appears to be fairly linear over the narrow range of the data.

7.2 An Empirical Model for Drag vs. Roughness

We now attempt to develop a mathematical model for the drag coefficients as a function of roughness, and along this line three key questions now present themselves:
1) What is the suitable form for such a model? That is, are roughness height parameters the only important quantities affecting drag or are wavelength parameters important as well? The waviness results show that

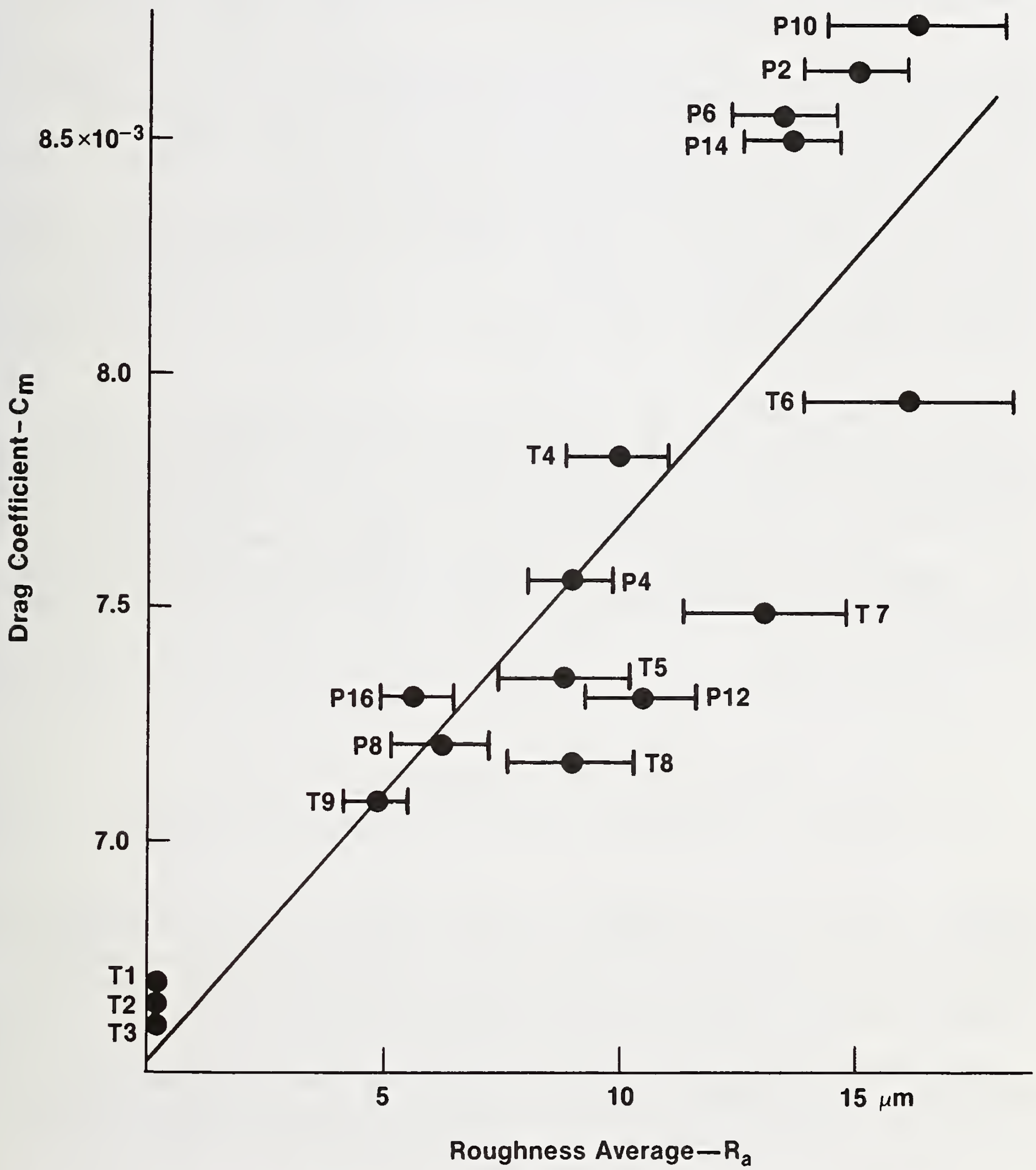

Figure 20. C_m vs. R_a showing fitted straight line. The uncertainties in R_a are derived from Tables 2 and 3, column 5.

roughness wavelength must have some importance because the long wavelength, structural waviness properties seem to affect the drag very little, whereas the short-wavelength microroughness had a significant effect. For example, the peak-to-valley waviness of disk T-1 is quite large. If we assume that the waviness profile is approximately sinusoidal, then we can estimate a value for the R_a of the waviness profile based on peak-to-valley waviness measurements. For a sinusoidal profile, R_a is equal to the peak-to-valley height divided by π . Since the average peak-to-valley waviness height is equal to ~445 μm (table 9), we estimate that R_a is equal to 142 μm, an order of magnitude larger than the R_a values measured by the stylus. Yet the drag coefficient of T-1 is almost identical to those of the other lapped disks; therefore, it seems that any effects of waviness height are mitigated by the fact that the characteristic waviness wavelength (~360 mm) is much longer than roughness wavelengths. We would like for the model to account for this insensitivity of the drag coefficient to waviness.

2) Is R_a or R_{max} a more important parameter for drag? We leave R_q out of this discussion because it is evident from equations 1 and 3 that R_a and R_q are very similar parameters and that there would be little to choose between them.

3) Can the same model be used to characterize both the Ti alloy disks and the painted disks?

The above questions are handled by using the method of least squares, a statistical technique for measuring the goodness of fit of a mathematical model to a set of data. Given a set of N data points $y_i(x_i)$ that depict the relationship between a dependent variable y and an independent variable x and a model y(x) involving p estimable parameters, $a_1,\ldots,a_p$, the best model is the one that minimizes the residual standard deviation RSD of the data points about the fitted curve. RSD is given by

$$\mathrm{RSD} = \left[\sum_{i=1}^{N} \frac{(y(x) - y_i(x_i))^2}{D} \right]^{1/2} , \qquad (15)$$

where D is equal to the degrees of freedom (N-p) of the fit. The smaller the RSD, the more credible the fit. The statistical calculations for fitting the data to the models were done using the computer software package, DATAPLOT, developed by Filliben and described elsewhere [34,35].

In order to answer the first question, we consider three empirical models for the dependence of C_m on roughness and wavelength. These are

Model 1: $C_m = aR_a + C_o$,

$$\text{Model 2:} \quad C_m = bR_a/(\lambda_{pc})^{1/2} + C_o, \text{ and} \tag{16}$$

$$\text{Model 3:} \quad C_m = cR_a/\lambda_{pc} + C_o.$$

These models assume a linear dependence of C_m upon R_a but account for the effect of the peak-count wavelength λ_{pc} in different ways. In all of them, however, the constant C_o represents the drag coefficient expected for a hydrodynamically smooth disk where the roughness effects are so small as to be negligible.

Model 1 does not admit any wavelength dependence at all. It assumes that the drag coefficients depend only on the heights of the surface asperities without regard to their separation. This might be a good model under the limited range of roughness and C_m shown in figure 20, but it clearly breaks down for the long-wavelength asperities of the waviness regime. Model 3 assumes a linear dependence of C_m on the quantity R_a/λ_{pc}. Since this quantity can be thought of as a measure of the surface slopes over the sampling length of 7.6 mm, the model assumes that C_m is primarily a function of the slope of the surface with respect to the average flow direction. A plot of the data for C_m vs. R_a/λ_{pc} is shown in figure 21, and indeed, the data seem to fit a straight line slightly better than do the C_m vs. R_a data of figure 20. Model 2 is a compromise between the other two. It postulates a dependence of C_m on both roughness and wavelength, but the dependence on roughness is the more significant. The C_m data are plotted vs. $R_a/(\lambda_{pc})^{1/2}$ in figure 22. Here again, the data seem to approximate a straight line better than do those of figure 20.

The data were fitted to the three models in turn using the DATAPLOT program previously mentioned. Each of the 17 data points was weighted equally in the fitting procedure, and, with 2 adjustable parameters for each model, there are 15 degrees of freedom. Results obtained for a, b, c, C_o and the residual standard deviations (RSD) are shown in table 11,

Table 11. Results of Fitting Three Models to the Data for C_m vs. R_a.[a]

Model $C_m=$	C_o $\times 10^{-3}$	a,b,c	RSD $\times 10^{-4}$
$aR_a + C_o$	6.53 ± 0.16	$1.15 \pm 0.15\times10^{-4}$ μm^{-1}	3.28
$bR_a/(\lambda_{pc})^{1/2} + C_o$	6.48 ± 0.07	$3.85 \pm 0.22\times10^{-3}$ μm$^{-1/2}$	1.60
$cR_a/\lambda_{pc} + C_o$	6.60 ± 0.10	0.105 ± 0.009	2.19

[a]The uncertainties are standard deviations obtained from the least squares fitting routine [34,35].

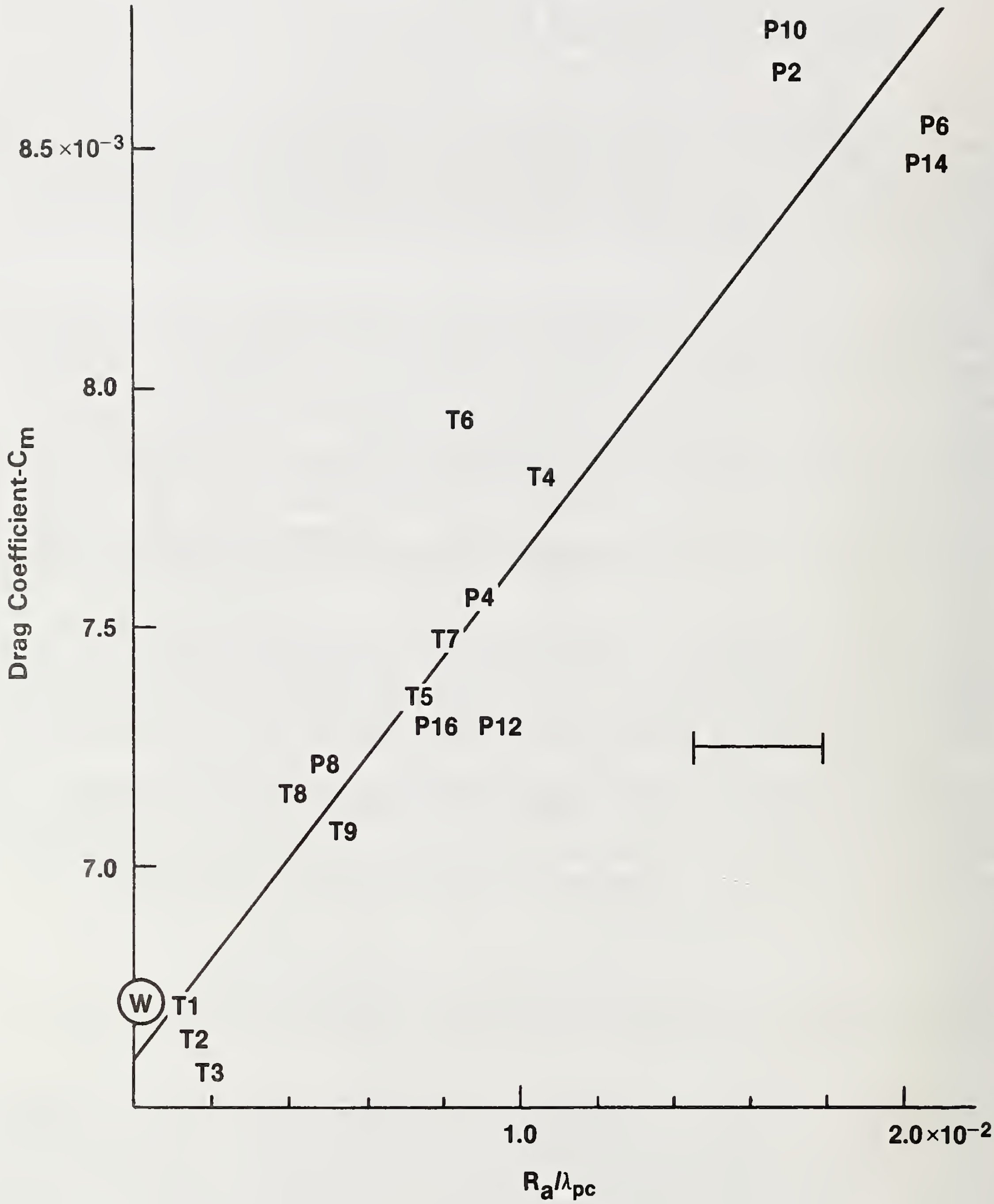

Figure 21: C_m vs. R_a/λ_{pc} with fitted least squares straight line. The horizontal bar shows a typical uncertainty for R_a/λ_{pc}. The point W was obtained from the waviness data of disk T-1.

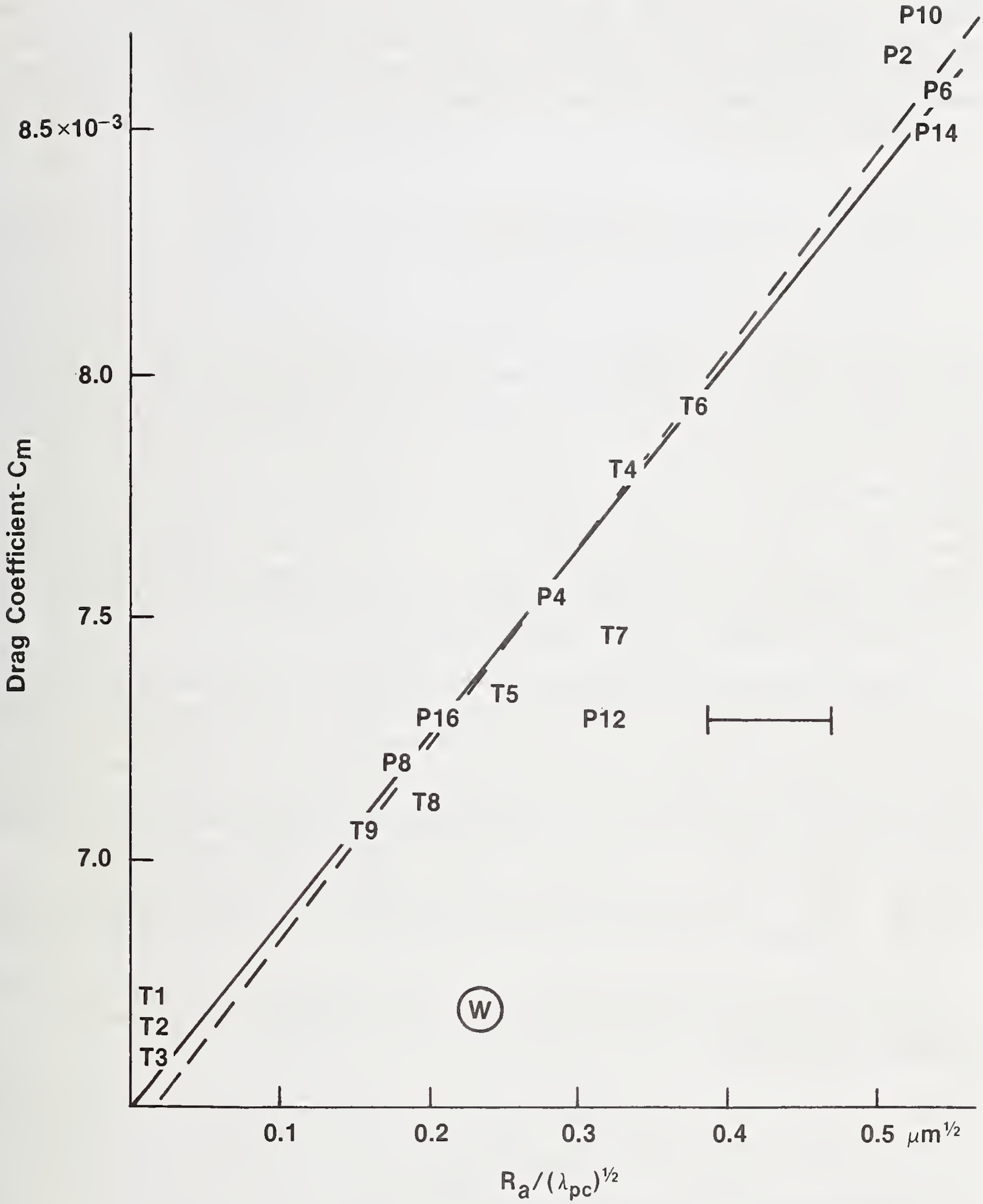

Figure 22. C_m vs. $R_a/(\lambda_{pc})^{1/2}$ with fitted least squares straight lines. The point W was obtained from the waviness data of disk T-1.

and the best lines are the ones plotted as solid lines in figures 20-22. Model 2 fits the data best since it has the smallest RSD. To get an idea of how significant this result is, we calculated the F ratio [36], a statistic that can be used for comparing the fits of various models to data. If, for example, we wish to compare Model 1 with Model 2, the ratio F_{12} is given by

$$F_{12} = (RSD_1)^2/(RSD_2)^2 = 4.2 \tag{17}$$

Then with a value for F_{12}, we can use statistical tables [37] or computer software statistics packages such as DATAPLOT [34,35] to obtain the probability P_F for F_{12} to exceed 4.2, given the assumption that both models are equally correct. P_F is a function not only of F but of the degrees of freedom of the two models, in this case 15 for each. The corresponding entry in the statistical tables is $P_F(F, 15, 15)$. For Model 1 vs. Model 2, P_F is equal to 0.4 percent, a result which suggests that Model 1 is an unlikely choice. To state it more specifically, if Model 1 and Model 2 were equally good choices, there would be only a 0.4 percent probability that $(RSD_1)^2$ would exceed $4.2(RSD_2)^2$. Model 2, therefore, looks significantly better than Model 1.

There is little to choose, however, between Models 2 and 3. The ratio F_{32} is 1.9. The corresponding P_F value of 11 percent suggests that Model 2 is the likelier choice, but this conclusion get modified when one takes the waviness data of disk T-1 into account. As before, we assume that disk T-1 has an effective waviness average R_a of 142 μm and an effective λ_{pc} of 360 mm and that waviness affects drag according to Models 2 or 3. When we plot the C_m value of 6.7×10^{-3} for disk T-1 versus $R_a/(\lambda_{pc})^{1/2}$ and R_a/λ_{pc}, we get the points labeled W on figures 21 and 22. Then, if these points W are included in the least squares fits, the RSDs are almost equal, 2.3×10^{-4} for Model 2 and 2.1×10^{-4} for Model 3.

Now, we turn to the question of whether R_a or R_{max} is the more significant roughness height parameter for disk drag. We therefore consider the models

$$\begin{aligned}
&\text{Model 2a:} \quad C_m = bR_a/(\lambda_{pc})^{1/2} + C_o, \\
&\text{Model 2b:} \quad C_m = b_1 R_{max}/(\lambda_{pc})^{1/2} + C_o, \\
&\text{Model 3a:} \quad C_m = c R_a/\lambda_{pc} + C_o, \text{ and} \\
&\text{Model 3b:} \quad C_m = c_1 R_{max}/\lambda_{pc} + C_o,
\end{aligned} \tag{18}$$

and we fit these to the data with the W points either included or excluded in the fit. For all of these cases, the RSD values are not significantly changed by the use of R_{max} instead of R_a; therefore, it appears that R_a and R_{max} are equally good parameters. Since R_a is the more widely used of the two parameters, it seem that Models 2a and 3a are more convenient than 2b and 3b.

Lastly, we face the question of whether the painted disks and the titanium alloy disks require different models or whether it is reasonable to use a single model as we have been doing. This type of question has been addressed directly by Neter and Wasserman [38], whose approach we follow here. Using Model 2 for the moment, straight lines are fitted in turn to the Ti alloy disk data only, to the painted disk data only, and finally to all of the data. The results for the parameters are shown in table 12. Then, an F statistic is calculated from the residual sums of squares (RSS) of the three fits, where

$$RSS = RSD^2 \times D. \tag{19}$$

The formula for F and the result of 1.68 are shown in table 12. To find out whether this value of F is reasonable, we obtain the probability P_F for obtaining a value of F larger than 1.68 assuming that the single model with 15 degrees of freedom is the correct description. This probability corresponds to the entry P_F (1.68,2,13) [38] in the statistical

Table 12. Testing the Equivalence of the Painted and Ti Alloy Disk Data for the Model:

$$C_m = b\ R_a/(\lambda_{pc})^{1/2} + C_o$$

Data Set	b $\mu m^{-1/2}$ $\times 10^{-3}$	C_o $\times 10^{-3}$	D	RSD $\times 10^{-4}$
Ti Alloy (T)	3.33 ± 0.28[a]	6.57 ± 0.06	7	1.14
Painted (P)	4.28 ± 0.46	6.32 ± 0.19	6	1.89
All	3.85 ± 0.22	6.48 ± 0.07	15	1.60

$$F = \frac{\{RSS(all) - [RSS(P) + RSS(T)]\}/\{D(all) - [D(P) + D(T)]\}}{[RSS(P) + RSS(T)]/[D(P) + D(T)]} = 1.68$$

[a]The uncertainties are standard deviations obtained from the DATAPLOT least squares fitting routine [34,35].

tables. The result of 22 percent indicates that the use of a single model for all disks is reasonable. The same hypothesis has been tested using the R_a/λ_{pc} model and the probability P_F is 39 percent.

7.3 Final Working Model

We are left with two reasonable models for describing the drag of disks as a function of roughness. At present, there does not seem to be any physical reason why one should be chosen over the other. Since the $R_a/(\lambda_{pc})^{1/2}$ model fits the data better when the odd W point is excluded, it perhaps should be chosen as the more reasonable one in the microroughness regime we have been studying. It may be that subsequent experiments will determine that the exponent of λ_{pc} is actually some fractional value other than 1/2. We have done some preliminary calculations along these lines, i.e. we have fit the data to a model of the form $R_a/(\lambda_{pc})^k$, where k is an adjustable exponent. The best values for k vary between 0.4 and 1.0, depending on whether the R_{max} or R_a data are used in the model and on whether the painted or Ti disk data sets are studied. Therefore, for the present, we relate the disk drag coefficients to roughness by the simpler model:

$$C_m = [3.85\ R_a/(\lambda_{pc})^{1/2} + 6.48]\times 10^{-3}. \tag{20}$$

The above numerical results were checked by the inverse fitting procedure, that is, the quantity $R_a/(\lambda_{pc})^{1/2}$ was taken as the dependent variable and C_m was taken as the independent variable. Although the relationship, $R_a/(\lambda_{pc})^{1/2} = a_1 C_m + a_o$, is awkward to interpret physically, this procedure is more correct statistically because the scatter in the $R_a/(\lambda_{pc})^{1/2}$ data was significantly larger than the scatter of 0.8 percent in the C_m data, and the dependent variable should be the one with the larger associated uncertainties. The best line which results from this inverse fitting procedure is shown as the dashed line in figure 22, and the fitted parameters are $C_o = 6.43 \times 10^{-3}$ and $b = 4.04 \times 10^{-3}\ \mu m^{-1/2}$. Both of these are within one standard deviation of the original values given in equation 20. We could use the later result as the final model, but it does not seem as physically realistic as the model given in equation 20 for the following reason. Disks T-1, T-2, and T-3 were expected to be hydrodynamically smooth and the close agreement in the measured drag results from these disks suggests that the model should not dip too far below these points, and correspondingly, that the intercept should be close to 6.6×10^{-3}. Hence, we conclude that equation 20 is the better model for disk drag vs. roughness under the experimental conditions that were used.

The functional form represented by equation 20 is only one of many that could be chosen to describe disk drag, and it is strictly an empirical one. A more physically meaningful form might look like the following

$$C_m = a(R_a - R_o)e^{-\lambda_{pc}/\Lambda} + C_o, \quad R_a > R_o,$$
$$C_m = C_o \qquad\qquad , \quad R_a \leq R_o, \tag{21}$$

where R_o is the maximum admissible R_a for a hydraulically smooth surface, C_o is its corresponding drag coefficient, Λ is a horizontal length scale factor, a is an adjustable parameter, and all of the aforementioned quantities would depend on the disk Reynold's number. Such a model, however, is probably too elaborate for the limited range of data taken during this experiment.

The present model was derived for only a single rotational speed with Reynold's number 1.5×10^6, and at this rotational speed the outer edges of the disk have a speed of approximately 18m/s (comparable to a ship speed of ~36 knots). Under these conditions, the maximum peak-to-valley roughness for which the surface is considered to be a hydraulically smooth surface is estimated to be 5.6 μm according to a formula discussed by Schlichting [39]. If this peak-to-valley roughness of 5.6 μm corresponds to R_{max}, the R_{max}/R_a ratios from table 6 can be used to estimate the maximum admissible R_a for a hydraulically smooth disk under these conditions. The value falls between 0.6 and 1.2 μm, a result which suggests that at a Reynold's number of 1.5×10^6 the smooth disks, T-1, T-2, T-3, were hydraulically smooth, but the others were not.

8. Conclusions

Stylus measurements have been performed on a number of painted and machined rotating disks, and from these a number of statistical parameters have been derived for describing the microroughness surface topography. We have tried to simplify the difficult theoretical problem of relating skin-friction fluid drag to surface topography by postulating that the drag coefficient C_m is a simple function of the average roughness R_a and a wavelength parameter which we call the peak-count wavelength λ_{pc}. The model,

$$C_m = bR_a/(\lambda_{pc})^{1/2} + C_o, \tag{22}$$

fits the data quite well and can be used to make quantitative predictions of C_m for disks from a knowledge of these two roughness parameters.

In this experiment, a specific correlation has been drawn between the roughness and the hydrodynamic drag of rotating disks. In addition, the present experiment has modelled the effect of roughness wavelength, as well as roughness amplitude, on drag and has formulated the parameter λ_{pc} to characterize the wavelengths of random surfaces. Previous studies of drag vs. roughness include those by Townsin, et al. [40], Karlsson [41], and Musker and Lewkowicz [42] on flat plates, and that by Lackenby [1] on full scale ships, and the work of Nikuradse, Schlichting and others [39] on rough pipes.

The empirical and theoretical limitations of the mathematical model are considerable, however. First, the model was derived for only one angular speed. Belt and Smith [31] measured the drag of these same disks as a function of speed, however, and their straightforward data suggest that the model can be extended to a range of speeds fairly simply with the addition of one or two parameters. Second, the study was limited to the microroughness caused by machining marks and paint texture. Even in this regime, the dependence of drag upon roughness is quite significant. Although some measurements of waviness were done to characterize the structural roughness of the disks, the relative importance of the macroroughness regime should be studied by fabricating and testing disks with significant macroroughness and comparing the results with those of the present study. Finally, similar experiments need to be performed on larger objects, such as plates and ships, to determine how significant the effects of the microroughness are to the operation of naval and commercial vessels in the light of the other surface degradation effects on the macroroughness.

The theoretical problem is so complex that the proposed models are based on intuitive ideas about what the most pertinent quantities might be, rather than on a fundamental knowledge of fluid dynamical processes. Theoretical efforts probably should be concerned with relating the characteristic roughness height and wavelength parameters to characteristic scale parameters of the fluid flow, such as the mixing length and the scale of turbulence. As to surface topography, one can learn a great deal by characterizing the surfaces with two simple height and wavelength parameters, like R_a and λ_{pc}. At the present state of knowledge, the key to the problem is not to find the optimum surface parameters affecting drag, but rather to relate straightforward height and wavelength parameters to drag by a valid physical model. R_a is a convenient choice because it is the most widely used surface height parameter. The quantity λ_{pc} can be related to the peak count parameter used by engineers and surface metrologists. By contrast, the traditional use of the parameters MAA and K_s is fairly restricted to hydrodynamicists.

In future experiments, some analysis of the power spectral density will be needed to sort out the relative effects of the microroughness and macrogroughness regimes on drag, and eventually if the physical models become more complete, it is possible that other statistical functions may be needed to characterize the surface adequately.

9. Acknowledgments

The authors are grateful to H. S. Preiser and D. R. Laster for their original suggestion of this work and for their support and encouragement along the way; to J. J. Filliben, S. Leigh, and K. R. Eberhardt for their guidance with the statistical calculations; to B. Borchardt, D. R. Flynn W. Liggett, and P. Purtell for their careful reading of the manuscript; and to S. Morris for assistance in its preparation. We would also like to acknowledge enlightening discussions with G. Belt, A. Ticker, E. Neal, and N. Smith. This work was supported mainly by the David Taylor Naval Ship Research and Development Center under contracts N00167-78-WR8-208 and N00168-79-WR7-0183.

10. References

1. H. Lackenby, Proc. Instn. Mech. Eng. 176, 981 (1962).

2. D. R. Laster, H. S. Preiser, and E. Neal, private communication (Apr., 1979).

3. H. Schlichting, Boundary-Layer Theory, 7th edition, trans. J. Kestin (McGraw-Hill, New York, 1979).

4. R. L. Townsin, J. B. Wynne, A. Milne, and G. Hails, in 4th Int. Cong. on Marine Corrosion and Fouling (Centre de Recherches et d'Etudes Oceanographiques, Boulogne, 1976) p.23.

5. P. S. Granville, Similarity-Law Characterization Methods for Arbitrary Hydrodynamic Roughness, DTNSRDC Report 78-SPD-815-01 (Feb., 1978).

6. J. A. Malone, M. M. Murtagh, M. J. Ailman, K. D. Baetsen, and D. E. Little, Ship Roughness Technology Program, Vol. I, Dept. of Commerce Report MA-RD-930-81014 (Oct., 1980). Although we use the same terminology as those authors, we have redefined the three roughness regimes slightly.

7. T. R. Thomas and R. S. Sayles, Mecanique Materiaux Electricite No. 337, p. 7 (Jan. 1978).

8. D. G. Chetwynd, Wear 57, 137 (1979).

9. E. C. Teague, Evaluation, Revision, and Application of the NBS Stylus/ Computer System for the Measurement of Surface Roughness, NBS Tech. Note 902 (U.S. Dept. of Commerce, Wash., D.C., 1976).

10. T. V. Vorburger, E. C. Teague, and F. E. Scire, Dimensions/NBS 62, No.11, 18 (Nov. 1978).

11. D. J. Whitehouse, in Characterization of Solid Surfaces, ed. P. E. Kane and G. R. Larrabee (Plenum, New York, 1974) chap. 3.

12. J. Peklenik, Proc. Instn. Mech. Engrs. 182 Pt 3K, 108 (1967-68).

13. R. S. Sayles and T. R. Thomas, Trans. Am. Soc. Mech. Engrs. F: J. Lub. Tech. 101, 409 (1979).

14. D. J. Whitehouse, Pro. Instn. Mech. Engrs. 192, 179 (1978).

15. American National Standards Institute B46.1-1978, Surface Texture (American Society of Mechanical Engineers, New York, 1978).

16. J. M. Elson and J. M. Bennett, J. Opt. Soc. Am. 69, 31 (1979).

17. J. Jungles and D. J. Whitehouse, J. Phys. E. 3, 437 (1970).

18. T. V. Vorburger, E. C. Teague, F. E. Scire, and F. W. Rosberry, Wear 57, 39 (1979).

19. H. Hacking, Int. Ship Painting and Corrosion Conf. (1974) p. 53.

20. Ref. 3, p. 615ff.

21. P. T. Manning, Wear 57, 365 (1979).

22. D. K. Brown, Proc. 5th Inter. Naval Corrosion Conf. (Defence Scientific Establishment, Auckland, New Zealand, 1976) p. 7.1.

23. R. C. Spragg and D. J. Whitehouse, Proc. Inst. Mech. Engrs. 185, 697 (1970-1).

24. Ref. 15, p. 27

25. P. S. Granville, J. Ship Res. 17, 181 (1973).

26. M. G. Natrella, Experimental Statistics, NBS Handbook 91 (Dept. of Commerce, Wash., 1963) p. 1-10.

27. S. Leigh and J. J. Filliben, private communication (Nov., 1980).

28. J. F. Allan and R. S. Cutland, Trans. N.E.C.I.E.S. 72, 257 (1955).

29. M. Kubo and J. Peklenik, CIRP Annals 16, 235 (1968).

30. Y. Tanimura, E. C. Teague, F. E. Scire, R. D. Young, and T. V. Vorburger, Bulletin of the Nat. Res. Lab. of Metrology (Japan) 30, 37 (1981).

31. G. S. Belt and N. A. Smith, Drag of Slimes and Smooth Surfaces as Measured by a Rotating Disk, DTNSRDC Report SPD-0865-01 (DTNSRDC, Bethesda, MD, July 1979).

32. G. S. Belt and D. R. Laster, private communication (Nov., 1978).

33. Ref. 3, p. 105f.

34. J. J. Filliben, in Proceedings of the Statistical Computing Section of the American Statistical Association (San Diego, 1978) p. 344.

35. J. J. Filliben, in Proceedings of the Twelfth Interface Symposium on Computer Science and Statistics (Univ. Waterloo, Waterloo, Canada, 1979) p. 147.

36. See, for example, P. R. Bevington, Data Reduction and Error Analysis for the Physical Sciences, (McGraw-Hill, New York, 1969) p. 196.

37. See, for example, B. Ostle and R. W. Mensing, Statistics in Research, (Iowa State University Press, Ames, Iowa, 1975) p. 545ff.

38. J. Neter and W. Wasserman, Applied Linear Statistical Models, (Richard D. Irwin, Inc., Homewood, Illinois, 1974) p. 160ff.

39. Ref. 3, p. 659.

40. R. L. Townsin, D. Byrne, A. Milne and T. Svenson, Naval Architect Sept. (1980) p. 459.

41. R. I. Karlsson, in Proc. Int. Symp. on Ship Viscous Resistance (SSPA, Gothenborg, 1978) p. 9:1.

42. A. J. Musker and A. K. Lewkowicz, in Proc. Int. Symp. on Ship Viscous Resistance (SSPA, Gothenborg, 1978) p. 11:1.

NBS-114A (REV. 2-80)

U.S. DEPT. OF COMM. **BIBLIOGRAPHIC DATA SHEET** (See instructions)	1. PUBLICATION OR REPORT NO. NBS TN 1151	2. Performing Organ. Report No.	3. Publication Date January 1982

4. TITLE AND SUBTITLE

Surface Roughness Measurements of Circular Disks and Their Correlation with Hydrodynamic Drag

5. AUTHOR(S)

T.V. Vorburger, F.E. Scire, and E.C. Teague

6. PERFORMING ORGANIZATION (If joint or other than NBS, see instructions)

NATIONAL BUREAU OF STANDARDS
DEPARTMENT OF COMMERCE
WASHINGTON, D.C. 20234

7. Contract/Grant No.

8. Type of Report & Period Covered

Final

9. SPONSORING ORGANIZATION NAME AND COMPLETE ADDRESS (Street, City, State, ZIP)

Sponsored in part by:
David Taylor Naval Ship Research and Development Center
Annapolis, MD 21402

10. SUPPLEMENTARY NOTES

☐ Document describes a computer program; SF-185, FIPS Software Summary, is attached.

11. ABSTRACT (A 200-word or less factual summary of most significant information. If document includes a significant bibliography or literature survey, mention it here)

The problem of relating hull roughness to the drag of ships is a complex and important one in ship research. One of the complications is that there are three fairly distinct roughness regimes (microroughness, macroroughness, and structural roughness) which make up a ship's surface and their relative importance is not yet well understood. The present report focuses on stylus measurements of the microroughness of rotating disks and their significant correlation with drag measurements. In particular, the roughest disks had drag coefficients C_m that were $\sim$30 percent greater than those of the smoothest disks. The following empirical formula was derived to relate C_m with the roughness average R_a and the peak-count wavelength λ_{pc} at a Reynold's number of 1.5×10^6.

$$C_m = bR_a/(\lambda_{pc})^{1/2} + C_o,$$

where $b = 3.85 \pm 0.22 \times 10^{-3}\ \mu m^{-1/2}$ and $C_o = 6.48 \pm 0.07 \times 10^{-3}$. The formula was observed to hold for both painted and bare metal disks.

12. KEY WORDS (Six to twelve entries; alphabetical order; capitalize only proper names; and separate key words by semicolons)

disks; drag; flow; friction disk; hulls; hydrodynamic drag; rotating disk; roughness; ships; stylus; surface roughness; surface topography

13. AVAILABILITY

☐ Unlimited
☐ For Official Distribution. Do Not Release to NTIS
☐ Order From Superintendent of Documents, U.S. Government Printing Office, Washington, D.C. 20402.
☒ Order From National Technical Information Service (NTIS), Springfield, VA. 22161

14. NO. OF PRINTED PAGES

63

15. Price

NBS TECHNICAL PUBLICATIONS

PERIODICALS

JOURNAL OF RESEARCH—The Journal of Research of the National Bureau of Standards reports NBS research and development in those disciplines of the physical and engineering sciences in which the Bureau is active. These include physics, chemistry, engineering, mathematics, and computer sciences. Papers cover a broad range of subjects, with major emphasis on measurement methodology and the basic technology underlying standardization. Also included from time to time are survey articles on topics closely related to the Bureau's technical and scientific programs. As a special service to subscribers each issue contains complete citations to all recent Bureau publications in both NBS and non-NBS media. Issued six times a year. Annual subscription: domestic $16; foreign $20. Single copy, $3.75 domestic; $4.70 foreign.

NOTE: The Journal was formerly published in two sections: Section A "Physics and Chemistry" and Section B "Mathematical Sciences."

DIMENSIONS/NBS—This monthly magazine is published to inform scientists, engineers, business and industry leaders, teachers, students, and consumers of the latest advances in science and technology, with primary emphasis on work at NBS. The magazine highlights and reviews such issues as energy research, fire protection, building technology, metric conversion, pollution abatement, health and safety, and consumer product performance. In addition, it reports the results of Bureau programs in measurement standards and techniques, properties of matter and materials, engineering standards and services, instrumentation, and automatic data processing. Annual subscription: domestic $11; foreign $13.75.

NONPERIODICALS

Monographs—Major contributions to the technical literature on various subjects related to the Bureau's scientific and technical activities.

Handbooks—Recommended codes of engineering and industrial practice (including safety codes) developed in cooperation with interested industries, professional organizations, and regulatory bodies.

Special Publications—Include proceedings of conferences sponsored by NBS, NBS annual reports, and other special publications appropriate to this grouping such as wall charts, pocket cards, and bibliographies.

Applied Mathematics Series—Mathematical tables, manuals, and studies of special interest to physicists, engineers, chemists, biologists, mathematicians, computer programmers, and others engaged in scientific and technical work.

National Standard Reference Data Series—Provides quantitative data on the physical and chemical properties of materials, compiled from the world's literature and critically evaluated. Developed under a worldwide program coordinated by NBS under the authority of the National Standard Data Act (Public Law 90-396).

NOTE: The principal publication outlet for the foregoing data is the Journal of Physical and Chemical Reference Data (JPCRD) published quarterly for NBS by the American Chemical Society (ACS) and the American Institute of Physics (AIP). Subscriptions, reprints, and supplements available from ACS, 1155 Sixteenth St., NW, Washington, DC 20056.

Building Science Series—Disseminates technical information developed at the Bureau on building materials, components, systems, and whole structures. The series presents research results, test methods, and performance criteria related to the structural and environmental functions and the durability and safety characteristics of building elements and systems.

Technical Notes—Studies or reports which are complete in themselves but restrictive in their treatment of a subject. Analogous to monographs but not so comprehensive in scope or definitive in treatment of the subject area. Often serve as a vehicle for final reports of work performed at NBS under the sponsorship of other government agencies.

Voluntary Product Standards—Developed under procedures published by the Department of Commerce in Part 10, Title 15, of the Code of Federal Regulations. The standards establish nationally recognized requirements for products, and provide all concerned interests with a basis for common understanding of the characteristics of the products. NBS administers this program as a supplement to the activities of the private sector standardizing organizations.

Consumer Information Series—Practical information, based on NBS research and experience, covering areas of interest to the consumer. Easily understandable language and illustrations provide useful background knowledge for shopping in today's technological marketplace.

Order the **above** *NBS publications from: Superintendent of Documents, Government Printing Office, Washington, DC 20402.*

Order the **following** *NBS publications—FIPS and NBSIR's—from the National Technical Information Services, Springfield, VA 22161.*

Federal Information Processing Standards Publications (FIPS PUB)—Publications in this series collectively constitute the Federal Information Processing Standards Register. The Register serves as the official source of information in the Federal Government regarding standards issued by NBS pursuant to the Federal Property and Administrative Services Act of 1949 as amended, Public Law 89-306 (79 Stat. 1127), and as implemented by Executive Order 11717 (38 FR 12315, dated May 11, 1973) and Part 6 of Title 15 CFR (Code of Federal Regulations).

NBS Interagency Reports (NBSIR)—A special series of interim or final reports on work performed by NBS for outside sponsors (both government and non-government). In general, initial distribution is handled by the sponsor; public distribution is by the National Technical Information Services, Springfield, VA 22161, in paper copy or microfiche form.

U.S. DEPARTMENT OF COMMERCE
National Bureau of Standards
Washington, DC 20234

OFFICIAL BUSINESS

Penalty for Private Use, $300

POSTAGE AND FEES PAID
U.S. DEPARTMENT OF COMMERCE
COM—215

U.S.MAIL

THIRD CLASS